Multi-scale modeling of automotive catalytic converters

by

Anton Fadic Eulefi

A thesis submitted in partial fulfillment of the requirements for the degree of

Master of Science

in

Chemical Engineering

Department of Chemical and Materials Engineering
University of Alberta

Abstract

In this work the Computational Fluid Dynamics modeling of the Automotive Catalytic Converter is comprehensively performed, including the study of the Flow Field distribution and the Temperature distribution under cold, non-reacting flow for six different monolith properties. A sensitivity study of some key lengths values was also performed. Later, the effect of the reactions is included by using an example reaction of Ammonia oxidation, which by the use of the multi-scale lookup tables technique allows to model the sub-grid effects of diffusion into the washcoat, that otherwise would be impossible to consider properly with alternatives modeling approaches.

Preface

Parts of the research conducted in this thesis corresponds to the work made by Dr. Teng-Wang Nien, who provided the look-up tables used to compute the source terms for the chemical reactions in Chapter 4.

Chapter 3 has been published as R.E.Hayes, A.Fadic, J.Mmbaga and A.Najafi. CFD modeling of the automotive catalytic converter. *Catalysis Today,* 188(1): 94 – 105, 2012. I was responsible for the coding of the simulations, the literature review and pre and post-processing of the information. A. Najafi initiated the study of the whole scale simulation of this kind of devices using CFD in the group. J.Mmbaga provided support to coding and R.E. Hayes provided guidance in theoretical aspects.

Chapter 4 has been published as A.Fadic, T.Nien, J.Mmbaga, R.E.Hayes and M.Votsmeier. A case study in multi-scale model reduction: The effect of cell desnity on catalytic converter performance. *The Canadian Journal of Chemical Engineering,* 92(9): 1607-1617, 2014. I was responsible for the coding of the simulations, the literature review and pre and post-processing of the information. J.Mmbaga provided assistance to coding. T. Nien provided the lookup-tables for computing the source terms. M.Votsmeier provided ideas to expand the original scope and R.E. Hayes provided guidance in theoretical aspects.

To my dad

Acknowledgments

First I would like to acknowledge my supervisor prof. Robert E. Hayes, whose support was essential on my pursuit of graduate studies, first by accepting me as an intern in the, rather cold, winter of 2011, while I was still an Undergrad in Chile, and later when I decided to pursue the Master's degree in 2012. His ideas, comments and support have been of critical importance for my studies.

Also I appreciate a lot all the comments, very original ideas and the motivation of Dr. Martin Votsmeier from Umicore, who helped me to increase the quality of my work in many aspects. Also, I am very grateful of him for giving me the chance of going to Germany and spending some of the time at the TU Darmstadt, working in collaboration with the prof. Vogel's of Technical Chemistry research group and also with the Umicore Automotive Catalyst group.

I would also like to acknowledge Dr. Joseph Mmbaga, who introduced me into the CFD world, sharing tutorials, tips and tricks and most importantly, having enough patience, of which I am really grateful because it was necessary, especially when I started. In the same regard, I would like to acknowledge Dr. Rajab Litto, whose help and kindness have always been present.

Also I would like to acknowledge the now Dr. Teng-Wang Nien, whose help and support has been of the utterly importance in this work.

I would like to acknowledge all the people I've met in Germany while working at the TU Darmstadt and from whom I learned a lot, academically and personally. I acknowledge Markus Klingenberger, from whom I've got the motivation to learn how to code using MATLAB. Also I acknowledge Artur Vizer, whose comments, ideas and discussions where beneficial directly and indirectly to this work.

Finally, I would like to acknowledge all the friends I have made in Edmonton and Darmstadt, with whom I shared good times and it helped me as a good distraction for the leisure time.

Contents

List of Figures

List of tables

Nomenclature	
ρ	Density, fluid
u_i	Velocity vector
∂_i	Gradient operator
P	Pressure
τ_{ij}	Stress tensor
b_i	Body force
δ_{ij}	Kronecker delta
μ	Viscosity
T	Temperature, fluid
$\dot{S}$	Source term
D_b	Bulk diffusion
$D_{a,eff}$	Effective axial dispersion
D_h	Hydraulical diameter
K_{ax}	Permeability, axial direction
k_{rad}	Permeability, radial direction
$C_{p,f}$	Thermal capacity, constant pressure, fluid
$C_{p,s}$	Thermal capacity, constant pressure, solid
k_s	Thermal conductivity, solid
Nu	Nusselt number
h	Convective heat transfer coefficient
a_v	Area to volume ratio
ΔH_r	Heat of reaction
R_i	Reaction rate
Re	Reynolds number
k	Turbulence kinetic energy
ε	Dissipation rate
ω	Specific dissipation rate
ϕ	Porosity
GHSV	Gas Space Hourly Velocity
CPSI	Cells per square inch

Chapter 1

1 Introduction

At the moment this thesis was written, awareness for the environment has been a topic of public concern in many countries and consequently more strict regulations regarding emissions that contribute to air pollution from different sources have been created by governments. However, it is not uncommon that the legislations have been performed somewhat independently with respect to the development of the technology, and as a consequence it has been increasingly more di cult for manufacturers to find more efficient devices that can fulfill these regulations. As an example, the newest norm to be launched in the European Union is the EURO VI, which is a framework that dictates the limits of pollutants that different mobile sources can produce to be commercially available in the European Union. The only two vehicles left out of this normative are airplanes and seagoing ships. The norm limits the production of Total Hydrocarbons (THC), Non-Methane Hydrocarbons (NMHC), Nitrogen Oxides (NO_x) and Carbon monoxide (CO). Table 1.1 is included to show the evolution of the Euro norm.

Table 1.1: European emission standards for passenger cars (Category M), g/km

Tier	Date	CO	THC	NMHC	NO_X	$HC+NO_X$	PM
Diesel							
Euro 1	July 1992	2.72	-	-	-	0.97	0.14
Euro 2	January 1996	1.0	-	-	-	0.7	0.08
Euro 3	January 2000	0.64	-	-	0.5	0.56	0.05
Euro 4	January 2005	0.50	-	-	0.25	0.30	0.025
Euro 5	September 2009	0.50	-	-	0.18	0.23	0.005
Euro 6	September 2014	0.50	-	-	0.08	0.17	0.005
Gasoline							
Euro 1	July 1992	2.72	-	-	-	0.97	-
Euro 2	January 1996	2.2	-	-	-	0.5	-
Euro 3	January 2000	2.3	0.2	-	0.15	-	-
Euro 4	January 2005	1.0	0.1	-	0.08	-	-
Euro 5	September 2009	1.0	0.1	0.068	0.06	-	0.005
Euro 6	September 2014	1.0	0.1	0.068	0.06	-	0.005

The main motivation of this work is the lack of comprehensive scientific literature regarding the full scale CFD modeling of the Automotive Catalytic Converter. This is a device widely used in cars and also other heavy duty equipment that work with a

combustion engine and it is needed to comply with the air polluting regulations. To be able to do this at the out low conditions of the engine, a catalyst is necessary because these reactions would not occur at an efficient rate without its presence.

To find better reactor designs, two different approaches can be used: physical experimentation and mathematical modeling. The former consists in developing a physical device to perform experiments and study the output of interests. Unfortunately, it has several disadvantages, namely the high cost related to the manufacture of the different physical models, the time and cost related to perform these experiments, the difficulties associated to repeatability, which sometimes is especially important when dealing with catalyst in the washcoat and it can be the case that there is a difficulty to measure some variables, like flow distribution, the concentration field, among others. On the other hand, this approach has always been important to validate and confirm the results of numerical simulations, and therefore despite its disadvantages it is still a necessary part of a complete study.

The second approach is in this case based on Computational Fluid Dynamics, which is used in different branches of engineering in which flow modeling is involved, for example in aeronautical engineering, naval engineering and chemical engineering, among others to model fluid flows by using computers. Some of the details of this method will be covered in the following section.

Numerical simulation possesses several advantages compared to physical experiments, for instance, it is very easy to change dimensions of the reactor and to change operating conditions, and therefore the cost of building different models is very low.

Another of its benefits is that all the conditions are known and they are controlled during the experiments, which sometimes is not easy to do when physical experiments are performed. Historically modeling has been used since the appearance of computers, but because of the magnitude of the needed resources, it has been restricted to certain applications.

Another of the most notable examples in this regard is the modeling of turbulence. This phenomenon is of extremely high interest in different areas of engineering, and therefore a considerable amount of work has been put in this topic. However, many areas are still not very well understood, and many semi-empirical relationships are employed to model, that have parameters fitted by physical experiments under certain conditions.

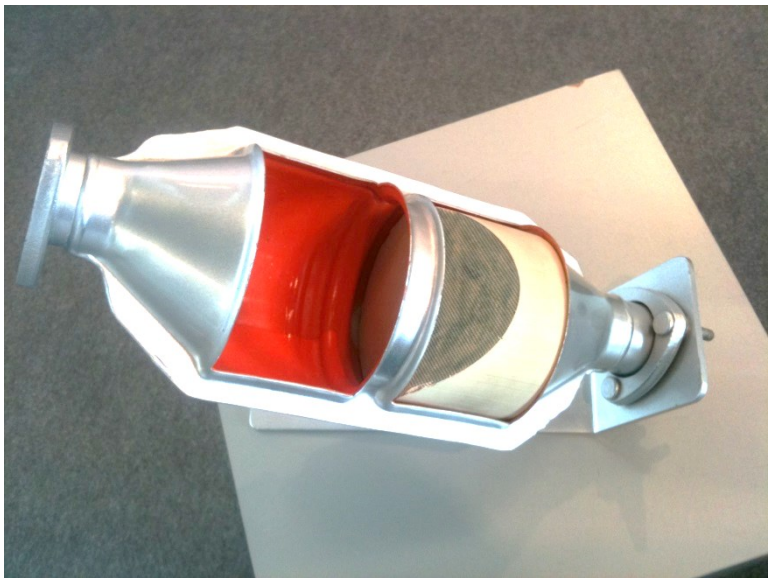

Figure 1.1: Picture of a catalytic converter showing the canning and the monolith.[1]

However, despite the impact that this has on the environment, the numerical simulation of this kind of reactor has not been performed thoroughly, mainly due to technological limitations such as the progress of the computing capability and, on the other hand, the development of the spline tools technology, which allows to efficiently model sub-grid effects by using lookup tables. More details on this topic are provided later on in this work. The multi-scale modeling can be observed in Figure 1.1, where the "macro-scale" of the reactor is the catalytic reactor itself, the "meso-scale" would be the channels of the monolith honeycomb and the "micro-scale" corresponds to the pores in the washcoat.

This thesis is organized as follows: the second chapter provides necessary background for chapters 3 and 4. In Chapter 3, a parametric study of the geometrical dimensions of the converter is performed and its effect on the flow field is studied. Also, some monolith properties are changed to study its effect on pressure drop and flow and temperature distribution. In Chapter 4, the study of different monolith configurations varying cell density and wall thickness is performed. In this chapter a complex mechanism is considered and it is accounted for diffusion into the washcoat. Finally, in Chapter 5 the conclusions and steps for further research are discussed.

[1] Own source

Chapter 2

2 Background

2.1 Introduction

CFD stands for Computational Fluid Dynamics. It is a branch of fluid mechanics that is devoted to the study of fluid flow by the use of computers and it was the main tool used in this project.

The process of CFD is shown on Figure 2.1. The first step is to determine what flow problem is considered, which includes the geometry of the problem. Afterwards the mathematical equations that govern the flow have to be stated. At the same time, the boundary conditions on all boundaries have to be stated. The general case governing equations are shown in the following section.

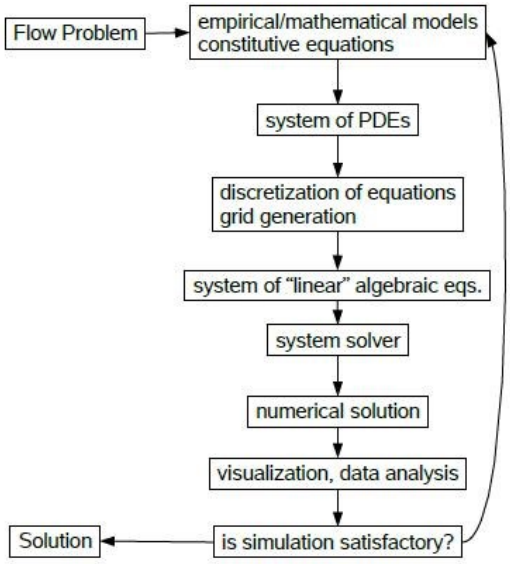

Figure 2.1: Solution process in CFD[2]

[2] taken from prof. Carlos Lange's MECE 539 lecture notes

2.2 Governing equations

Mass balance: From Fluid Mechanics, it is known that for the mass conservation to hold, the following has to be true:

$$\frac{\partial \rho}{\partial t} + \partial_i(u_i \rho) = 0 \tag{2.1}$$

Where ρ stands for the fluid density, u_j stands for the i component of the velocity and ∂_istands for the derivative in the i direction. In this work, the Einstein summation convention is used, by which the existence of the same index in two different, like in this case i, stand for the summation over that index.

Momentum balance: Also from Fluid Mechanics, following Newton's third law of motion the momentum balance can be derived and it is shown as follows:

$$\frac{\partial \rho u_j}{\partial t} + \partial_i(u_i u_j \rho) = -\partial_i P + \partial_i \tau_{ij} + b_j \tag{2.2}$$

The term τ_{ij} is called the stress tensor and it represents the forces producing shear on a differential face of the fluid. This term is not isotropic, which means that it is allowed for every face to have different magnitudes in all directions. *P* stands for the Pressure, which is also a force acting on the faces but it is always acting normal to the them and it always has the same value and the term b_j is called body force, which is a force acting on every part of the volume of the fluid. It can be for instance, the gravity force, or in this case it can be a fictitious force that models the effect of having a porous medium.

$$\rho \frac{\partial u_j}{\partial t} + u_i \partial_i(\rho u_j) = -\partial_i P + \partial_i \tau_{ij} + b_j \tag{2.3}$$

Angular Momentum balance: It is known that for the angular momentum to hold, the stress tensor τ_{ij} has to fulfill the following:

$$\tau_{ij} = \tau_{ji} \tag{2.4}$$

This equation only states that the stress tensor has to be symmetric, but does not provide any further information about the nature of it. Therefore, an assumption has to be made about it, in order of being able to use it in combination with the other terms of the momentum balance equation 2.3. One observation made from Newton, is that the shear stress is a linear function of the shear rate, which has been shown to be valid under many circumstances.

$$\tau_{ij} = \mu\left(\partial_i u_j + \partial_j u_i\right) - \frac{2}{3}\mu\delta_{ij}\partial_k u_k \tag{2.5}$$

Where μ is the constant of proportionality and is called viscosity, δ_{ij} is the operator Kronecker delta. If the fluid is incompressible, then the last term vanishes. This is the simplest approach by which the shear stress is modeled to be directly proportional to the shear rate. Different constitutive relationships exist. In the case of study, it is assumed that the fluid behaves as a Newtonian fluid, according to Eq. 2.4. In this work the viscosity is regarded as a function of the temperature, computed from the following polynomial t for air [2]:

$$\mu = -8.383\cdot 10^{-7} + 8.357\cdot 10^{-8}T - 7.694\cdot 10^{-11}\cdot T^2 + 4.644\cdot 10^{-14} * T^3 - 1.066\cdot -17T^4 \tag{2.6}$$

Energy balance: When the no heat exchange condition is dropped, the energy conservation principle has to hold. The equation that represents this is presented as follows:

$$\rho C_p \frac{\partial T}{\partial t} + \rho u_i \partial_i T = \partial_i(k\partial_i T) + \dot{S}_{other} \tag{2.7}$$

Where *T* is the temperature of the fluid, k is the conductivity of the fluid and finally $\dot{S}_{other}$ is a source term which includes heat generation or loss by chemical reaction and also in the modeling of the monolith, it accounts for the heat transfer between the fluid and the solid. Further on this is discussed in section 2.4.2. For the fluid phase, the heat conductivity is modeled as a function of the temperature, as follows [2]:

$$k_f = 1.679\cdot 10^{-2} + 5.073\cdot 10^{-5}T[\frac{W}{m}] \tag{2.8}$$

Mass transfer equation: When the pure fluid assumption is dropped, then a multi-component mixture exists and the effect of diffusion has to be included. Following Fourier's law of heat conduction, where heat flux is the proportional to a difference in temperatures with constant of proportionality k, there is an analogy for computing the mass flux, which is assumed to be proportional to the difference in concentrations, as follows:

$$J_i^j = -D_{eff}\partial_i C^j \tag{2.9}$$

Where D_{eff} is the effective diffusivity, analogous to the conductivity in the heat equation and C^j stands for the Concentration of species j. The minus sign indicates that the mass flux goes from higher concentrations to lower concentrations, being an exact analogy to heat transfer and temperature. However, in this case the diffusivity depends on what species is di using into which other, and therefore it is a matrix of diffusivities. When the mass flux is inputted into the mass transfer equation, it leads to the following:

$$\frac{\partial \rho Y^j}{\partial t} + \partial_i J_i^j + u_i \partial_i C^j = \dot{S}^j_{rxn,eff} \tag{2.10}$$

Where the second term on the left hand side is the mass transport by diffusion, the third term is the mass transport by convection and the right term is a source term, which accounts for chemical reactions for example, where mass is converted into other species. In Chapter 4, this term is the effective diffusion rate, which accounts for mass transfer limitations of washcoat diffusion. The bulk diffusion is modeled by the Fuller model [3] as a function of temperature, as follows [2]:

$$D_b = 1.0294^{-9} \cdot T^{1.75}[m^2/s] \tag{2.11}$$

Note that diffusion is not allowed in the radial direction, since the channel walls are porous, however they offer a big mass transfer resistance. In the axial direction, the diffusion can be approximated by the Taylor-Aris model [4] for laminar flow, where:

$$D_{a,eff} = D_b + \frac{(vD_h)^2}{192 D_b} \tag{2.12}$$

2.3 Boundary conditions

In the previous section the governing equations that determine the behavior of the variables of interest in the domain were shown. However, at the boundary (in physical systems it means at the physical boundaries and at the time boundary) the information has to be provided to determine the system of equations properly. It is understandable intuitively that the system of equations won't converge as expected due to its ill specification. In only certain cases, where the PDEs are of a specific form, it is possible

to solve the equations without some boundary conditions, but in the general case this can lead to convergence problems and once the whole is completely built it can be hard to assess where the error is. Also, in the boundary conditions the majority of the errors can be found, because they have influence they may have an impact on the whole domain an affect the value of the quantities of interest far from the boundary, and therefore the proper care has to be taken when setting them. Different name of boundary conditions exist for solving PDEs, but they can be classified in general as follows:

2.3.1 Dirichlet Boundary Condition

This boundary condition occurs when a prescribed value of any variable is set at the boundary of the form:

$$f(x_0) = f_0$$

Examples of this boundary condition in physical system are: prescribed temperatures at boundaries, prescribed mass flows or velocities at inlet or outlets and prescribed pressures, among others or in general, any information that is known directly of the system.

2.3.2 Neumann boundary Condition

This is a prescribed derivative, or more generally a gradient at a boundary, of the form:

$$\partial_i f(x)|_{x0} = f_0$$

Common uses of this kind of boundary condition are: specified heat fluxes (related to Fourier's Law in Heat Transfer), specified mass fluxes or symmetries, among others.

2.4 Modeling the effect of the monolith

Although the equations presented in the previous section hold to any single phase flow under the specified conditions, the effect of the monolith is not included specifically in them. Two different modeling strategies can be proposed, modeling the effect of the monolith by modeling every channel, as for example in [5], or by modeling the effect of the monolith assuming an average behavior and making use of the source terms of the equations previously stated. In this work, this is the approach that was used. First, some of the physical parameters of the monolith are described.

Cell density: This is the density of channels per surface area of the monolith. It is usually expressed in cells per square inch, CPSI. The most typical cell densities used in automotive applications are between 400 to 900 CPSI. This parameter has big impact in flow distribution, thermal properties and mass transport. The effect of the cell size is covered in this work.

Wall thickness: This is the thickness of the substrate, which has an impact on the thermal mass of the monolith. They are usually in the range of 0.1-2.0 mm.

Washcoat: This is a highly porous substance that covers the monolith walls. It contains the catalyst inside. The reactions take place inside this material.

Fluid volume fraction: This is the open area of the channel, where the flow can go through. This is the result of considering the cell density and taking out the substrate wall thickness and the washcoat wall thickness.

The physical parameters of for different monolith specifications can be found on Table 3.3.

2.4.1 Effect of the monolith on Continuity and Momentum equations

The effect on continuity equation is none. However, the effect of the monolith can be considered as an obstruction which is modeled by an anisotropic body force. The flow is known to be laminar in the channels, so it can be modeled combining the Darcy's law, which models the pressure drop through a porous medium and the Hagen-Poiseuille equation, which models the pressure drop through a cylindrical channel. By doing this, the pressure drop across the monolith can be computed as follows:

$$\partial_i P = -\frac{\mu \phi u_i}{K_{jk}} \delta_{jk} \tag{2.13}$$

and combing with the Hagen-Pousille flow, the parameter K can be computed as follows:

$$K = \frac{\phi D_h^2}{32} \tag{2.14}$$

It is worthwhile noting that for either a 2D or 3D simulation, the only component of the permeability tensor that can be modeled through 2.13 is the axial component. Therefore an assumption has to be made regarding the radial component of the permeability tensor. It has been reported in the literature [6] that assuming very low permeabilities in the radial direction forces the flow to go in the other direction, which in this case is the

radial direction. The radial component of the Permeability Tensor is modeled as follows [6]:

$$K_{rad} = K_{ax} \cdot 100 \tag{2.15}$$

Where K_{rad} is the radial component of the permeability tensor for either 2D or 3D simulations. In the simulations, the assumption 2.16 guarantees no radial flow inside the monolith zone. With this assumption, the source term, also called body force, in Equation 2.2 becomes:

$$b_j = -\frac{\mu u_j}{K_{ik}}\delta_{ik} \tag{2.16}$$

2.4.2 Heat modeling of the monolith

In the monolith section, another temperature variable is needed to account for the temperature of the solid T_s.

$$(1-\phi)\rho_s C_{p,s}\partial_t T_s = \partial_i k_{eff,s}\partial_i T_s + \dot{S}_{other} \tag{2.17}$$

The source term in this equation is related to the heat transfer between the solid and fluid phase and due to the heat produce due to the reaction. The convective heat transfer between the solid and the fluid is modeled by the Nusselt number, which is assumed to be 4 in this case [1], since it is a realistic approximation of assuming as boundary condition in the channel walls either constant heat flux or constant temperature [1]. This assumption is reasonable because the case of study does not have extremely large axial temperature gradients, which is a prerequisite for radiation to be significant [1].

$$Nu = \frac{hD_h}{k_f} \tag{2.18}$$

Where *h* is the convective heat transfer coefficient, D_h is the hydraulic diameter of a channel and k_f is the fluid conductive heat transfer. Finally, the convective component of the source term is modeled as follows:

$$\dot{S}_{convective} = ha_v(T_f - T_s) \tag{2.19}$$

Where h is the convective heat transfer coefficient and a_V is the area to volume ratio of a single channel. This is calculated using the fractional open frontal area, or porosity, of the monolith structure and the hydraulic diameter of the channels, as follows:

$$a_v = \frac{4\phi}{D_h} \tag{2.20}$$

The energy equation for the fluid phase is also altered because there is a source term in the fluid equation which is of the same magnitude but different sign of the aforementioned. The energy balance of the fluid has to be altered as well due to the porosity, as follows:

$$\phi\rho_f C_p \frac{\partial T_f}{\partial t} + \rho_f v_i \partial_i T_f = \partial_i (k_{eff} \partial_i T_f) + \dot{S}_{other} \tag{2.21}$$

The heat source due to the chemical reaction is computed as follows:

$$\dot{S}_{reaction} = \Delta H_r \cdot R_i \tag{2.22}$$

Where ΔH_r is the heat of reaction and R_i is the effective rate of reaction. The thermal conductivity of the monolith in the flow direction is computed as a weighted average of the washcoat fraction and its heat conductivity and the substrate fraction and its heat conductivity. The radial component of the heat conductivity is computed following the methods outlined in [7].

2.5 Turbulence and its modeling

2.5.1 The turbulence phenomenon

Turbulence represents a higher complexity challenge in terms of modeling. Up to date, only certain features of turbulence have been studied and understood thoroughly, being this the main cause of the difficulty to its modeling.

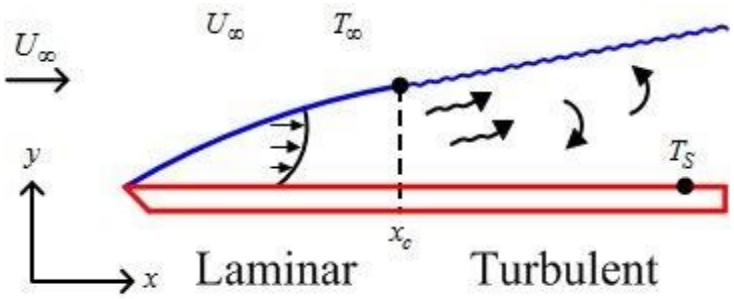

Figure 2.2: Illustrative sketch of flow over a plate.

Physically, it is shown on Figure 2.2. It is seen that when a fluid impacts a surface, first the flow is laminar, in which all molecules of fluid move in parallel layers. However, up to a certain distance downstream, some irregularities can be found regarding this behavior. In any case, the appearance of eddies is the characteristic property of turbulent flows.

Based on several experiments of flow in pipes, in 1883 Reynolds [8] showed that one single flow quantity can be used to determine whether the flow produces eddies or if it is laminar, named the Reynolds number:

$$Re = \frac{\rho u L}{\mu} \tag{2.23}$$

Where ρ is the fluid density, u is the free stream velocity, L is called the characteristic length and μ is the fluid viscosity. A flow can be characterized as turbulent just by its Reynolds's number. However, this classification is case dependent because in different situations, different ranges Re numbers can be found to state if a given flow is turbulent.

Summarizing, from Reynolds findings, turbulence is a phenomenon that occurs at high Re numbers, which means that occurs when the inertial forces are more relevant than the viscous forces and the magnitude that determines whether the flow is turbulent or not is case dependent, and usually has to be found experimentally.

2.5.2 Turbulence modeling

Regarding turbulence modeling, it is believed that no modification to Equation 2.6 is necessary to model turbulent flow, and this is the aim of DNS (Direct Numerical Simulation). However, the time and length scales of the turbulent eddies impose a harsh constraint for current computers, and this kind of approach is only used on

supercomputers. Extremely ne meshes and very small time steps would be necessary, which in practice make this approach impossible for engineering porpouses. When the laminar flow assumption is dropped, different more practical approaches from an engineering standpoint exist and are discussed in this section.

In this work it is only intended to provide an introduction of the terminology, methodology, advantages and disadvantages of some of the most used models in Engineering, and some concepts are provided for completeness of this work. For more in depth literature on turbulence, see [9].

RANS Models

One of the most popular approaches is the Reynolds Averaged Navier-Stokes, idea that was presented in Reynolds's [10] work of 1895 and characterizes a whole turbulence model family. The velocity can be separated in an average part and in a fluctuating part. When the Reynolds averaging process is undertaken, the following equation can be derived:

$$\frac{\partial \rho U_j}{\partial t} + \partial_i(U_i U_j \rho) = -\partial_i P + \partial_i[\tau_{ij} - \rho\langle u_i u_j\rangle] + b_j \tag{2.24}$$

In which 9 new terms appear, $\rho\langle u_i u_j\rangle$, although only 6 are independent and are called the Reynolds stresses. The problem comes when modeling this term because no information is known about it. This is known as the closure problem and for being one able to use this scheme some assumption or mathematical formulation has to be made about this term. Depending on the assumption to compute this term is what distinguishes the different RANS models.

The Boussinesq assumption: In 1877 Boussinesq [11] proposed that the momentum transfer caused by turbulent eddies can be modeled with an eddy viscosity. This is in analogy with how the momentum transfer caused by the molecular motion in a gas can be described by a molecular viscosity. The Boussinesq assumption states that the Reynolds stress tensor, $_{ij}$, is proportional to t strain rate tensor, and can be written in the following way:

$$-\rho\langle u_i u_j\rangle = \mu_t\left(\frac{\partial U_i}{\partial x_j}+\frac{\partial U_j}{\partial x_i}-\frac{2}{3}\frac{\partial U_k}{\partial x_k}\delta_{ij}\right)-\frac{2}{3}\rho k\delta_{ij} \tag{2.25}$$

The difference in this case is that the momentum transfer due to molecular viscosity is a property of the fluid, which means that the only information needed to capture the effect is to know what fluid is and its state variables. However, the transport of momentum due to turbulent viscosity is a property of the flow, which means that it will depend on the flow field as well. For a given fluid it is not sufficient information to determine the turbulent viscosity and therefore the parameter $_t$ has to be a function of the flow field. Conversely, the flow field is also depending on this parameter, as shown in Equation 2.22, expectedly, because the inclusion of turbulence has an effect on the flow field. One of the simplifying assumptions is that the quantity μ_t is isotropic. However, the most general case is that this property does not have the same behavior in different directions, due to asymmetric eddies and therefore if this assumption is made, a modeling error would be implied.

After considering the Boussinesq assumption, the next challenge is finding how to model the turbulent viscosityμ_t. Several models exist to do so, and they are classified mostly according to the number of extra equations needed to model this parameter. In this work, most of the emphasis is put on two equation models, so these are covered more in depth. Other models are included for completeness purposes only.

Zero and single equation models: Zero equation models are also known as algebraic models. These models are the simplest alternatives to model the turbulent viscosity, although they have reduced application because they were built for specific applications. One of the most popular examples of one equation models is the Spallart-Allmaras [12] model, which has been used mostly in aerodynamic flows.

Two equation models:

This kind of equation models includes several that have modifications.

$\boldsymbol{k-\varepsilon}$ **model:** The two transported quantities are turbulent kinetic energy, k, which is a measure of the intensity of the turbulence. The second transported quantity is $\boldsymbol{\varepsilon}$, which is a measure of the length scales of the eddies.

$$\partial_t(\rho k) + \partial_i(\rho k u_i) = \partial_j\left(\partial_j k \cdot [\mu + \frac{\mu_t}{\sigma_k}]\right) + P_k + P_b - \rho\epsilon - Y_m + S_k$$
$$\partial_t(\rho\epsilon) + \partial_i(\rho\epsilon u_i) = \partial_j\left(\partial_j k \cdot [\mu + \frac{\mu_t}{\sigma_k}]\right) + C_{1\epsilon}\frac{\epsilon}{k}(P_k + C_{3\epsilon}P_b) - C_{2\epsilon}\rho\frac{\epsilon^2}{k} + S_\epsilon \quad (2.26)$$

Once the field for these new variables is computed, the turbulent viscosity can be computed as follows:

$$\mu_t = \rho C_\mu \frac{k^2}{\epsilon} \quad (2.27)$$

The model has the following constants, showed on table 2.1.

Table 2.1: k-ε model parameters [13]

Parameter	Value
$C_{1\epsilon}$	1.44
$C_{2\epsilon}$	1.92
C_μ	0.09
σ_k	1.0
σ_ϵ	1.3

The k-ε model has several advantages over one or zero equations models, like for example better flow profile predictions and more versatility. However, it has been presented in the literature, that the model underperforms in certain cases, when there is flow separation or curved streamlines. To remedy some of these flaws, other models can be found in the literature. Most notably, the k-ω is presented as follows.

The k-ω model is based on Wilcox's [9] work. The transported quantities are turbulent kinetic energy k and specific dissipation rateω, which is also related to the length scales of eddies. The transport equations are presented in Equation 2.26.

$$\partial_t(\rho k) + \partial_i(\rho k u_i) = \partial_j\left(\partial_j k \cdot [\mu + \frac{\mu_t}{\sigma_k}]\right) + P_k - Y_m + S_k$$
$$\partial_t(\rho\omega) + \partial_i(\rho\omega u_i) = \partial_j\left(\partial_j \omega \cdot [\mu + \frac{\mu_t}{\sigma_k}]\right) + P_\omega - Y_\omega + S_\omega \quad (2.28)$$

The turbulent viscosity is computed as follows:

$$\mu_t = \alpha^* \frac{\rho k}{\omega} \quad (2.29)$$

The model's variables are similar to k model, however its parameters are different, but they are chosen by comparison against experimental data. Details about them, especially about the computation of are not provided due to length considerations, but they can be found in [9].

k-ω, with SST model: This model was developed by Menter [14]. The details can be found in the reference, but the most remarkable feature of this model is the use of blending functions, that makes the model go from a k in the far field to a k-ω close to walls. It is considered more stable and in the literature has been presented as a model with better predictions for flow separation, for example.

Other models

A vast amount of literature exists regarding different models for turbulence besides the RANS family models. Since it is out of the scope of this work, they will only be mentioned briefly.

LES Stands for Large Eddy Simulation and it is based on space-filtered equations. Time dependent calculations are performed. Large eddies are explicitly calculated. For small eddies, their effect on the flow pattern is taken into account with a sub-grid model of which many styles are available.

DES Stands for Detached Eddy Simulation. This model can be thought as a blend between a pure RANS model and a pure LES model, which switches between models depending on the presence of walls or depending on the turbulent length scale.

DNS Stands for Direct Numerical Simulation. As stated in section 2.5.2, the aim of this method is to solve the original Navier-Stokes equations without having to model independently the turbulence effects. For doing so, extremely ne meshes are required to model all the eddy scales and besides very small time steps are needed to capture the time dependent nature of turbulence. Therefore this method is extremely computational expensive, which prevents its usage in most engineering applications.

As a summary, many turbulence models exist and it is a matter of ongoing investigation. In general, the different approaches differ in terms on the scale of eddies that is resolved and the one that is modeled. DNS does not model any length scale, but is computationally expensive, which excludes it from many applications, especially for engineering purposes. On the other side, the simplest zero or one equation model have been tested for only certain applications.

2.6 Solving the equations

Given the complexity of the problem due to the type of equations, coupled system of non-linear PDE, and the complexity given by the different kind of geometries that are involved in modeling, it is impossible to solve these equations analytically for every single case with-out making some simplifying assumptions. Some teaching purpose examples can be solved by making use of this, but in general these are unrealistic and not suitable for engineering purposes. Therefore numerical methods have to be used to obtain a solution. The general strategy is to decompose the domain in simpler sections and apply the conservation equations in those sub domains. The problem becomes possible to solve, but the trade-o comes with the number of calculations necessary to solve these equations. Another issue that arises from using numerical methods is that an error is assumed in the domain decomposition, also called domain discretization or meshing, and it has to be assessed properly to make the solution meaningful. This topic is covered in more depth in section 2.7. The meshing has a big impact on the convergence of the solution. Also, with the turbulence models can have an impact on the way they behave.

2.6.1 Discretization methods

Once the domain has been discretized, the governing equations have to be computed based on this discretization. Three different methods exist:

Finite difference method

This is the simplest approach which only works on structured meshes. It is based on approximating the derivatives using based on a Taylor expansion of them. It has the advantage of being simple to code. However, currently it has very little application in CFD due to several reasons, among them, the requirement of a structured mesh, which is sometimes very hard to obtain, due to stability reasons and also because the error order induced by the method is higher than of the other two alternative methods.

Finite volume method

This method is based on computing fluxes from the original equation, which provides the characteristic of being conservative. It has the advantage of being applicable on structured and unstructured meshes, and it has been popular in CFD applications. Two of the most well-known available softwares use this method: Fluent and OpenFoam.

Finite element method

The unique characteristic of this method is the use of weighting functions. This method starts from taking the original equations and then converting them to the weak form, while weighting. The equations have to still hold on every element of the grid. The main idea is to find what weighting function would minimize the residual given by the integrated quantity, and therefore Calculus of variations is used to minimize the residual and to determine the weighting function. Comsol uses this discretization method, among others.

2.6.2 Available software

Since coding every single feature would be a time consuming activity, commercial and non-commercial codes have been developed to simplify the task of coding and to focus mainly in the physical modeling. This has had the approach taken by the industry because it simplifies and speeds up the process of research and development of the new technologies.

In this work, Comsol and Fluent codes were used. Comsol works on the Finite element method and Fluent on the Finite Volume Method.

2.7 CFD procedure

As shown in Figure 2.1 the process of solving these equations is iterative. This is due to the numerical approach of solving them that puts degrees of errors due to different sources in different steps. A well-known saying in CFD is "Garbage in equals garbage out". This is because of the different sources of errors that are described as follows:

Error assessment

The sources of errors made during simulating can be summarized in three, as follows:

$$\text{Total Error Source} = \text{Modeling} + \text{Numerical} + \text{User}$$

Modeling error

This source of error arises when one attempts to model the reality through a set of equations, boundary conditions and properties, described as follows:

Equation modeling: Some equations are thought to be exact, as for example mass and momentum conservation for single phase flow with no turbulence modeling. How-ever, because turbulence is a 3D, transient phenomenon with different length scales, it is known that very small element size would be needed and therefore coarser meshes are used with different turbulence models. Other possible sources are model assumptions, like ideal gas, non-compressible fluid and Newtonian fluid, among others.

Boundary conditions: This is related to unknown or uncertain boundary conditions, as for example when modeling heat, neglecting the effect of radiation, or assuming no flux of certain quantity where they are, for example.

Model parameters: This comes for example when unknown or imprecise data is inputted in the model. For example, regarding fluid properties it can be diffusivities, heat conductivities. Regarding the geometry, neglecting some features that can provide numerical difficulties and that are thought to have a very small effect on the solution. Finally, boundary condition parameters, as mass flows, temperatures, convective heat transfer coefficient, that are assumed either constant or with certain variations that do not correspond to the reality.

Numerical error

This error arises from solving the set of PDEs. There is the discretization error, which comes from making the grid, the residuals, or numerical error, which is a measure of how far is the numerical results from the exact solution. Since the exact solution is not known, it is compared substituting back the obtained fields in the equations and the deviation from the original equation is computed. Low residuals are no guarantee of a converged solution because the magnitude is chosen somewhat arbitrarily. To assess the grid error, mesh independence study is recommended, where certain key quantities are studied as a function of the mesh size, while preserving the underlying qualities of the mesh. To assess numerical error, key quantities are studied as well as a function of the convergence process. Once these quantities stabilize, and the residuals are low enough, it is a good indicator of a converged solution.

User error

This kind of error is the hardest to find. Since modeling is a human activity, mistakes can be made in the code that can be overseen and that can lead to unexpected results. Assessing this error can be quite cumbersome, and therefore the proper code assessment has to be done to check for this kind of errors.

Chapter 3

3 Flow Distribution Study

3.1 Introduction

In this section the numerical modeling of a catalytic converter is performed, focusing mainly on the effects on flow distribution when changes are performed to the geometry. Part of the work has been presented in [15].

Numerical simulation of catalytic converter has been a topic of interest because long time, although its usage has become more feasible only in recent years due to the increase of computing capability. Unfortunately there is no generally valid way of modeling the flow, mostly due to the effect of turbulence in the fluid flow. Currently there are investigations in this regard [16,17] that have become feasible due to the progress in computing capabilities.

Two are the main modeling approaches of automotive catalytic converter that can be found in the literature. One of them is the modeling of a single channel of the monolith [18,19]. This method has been of interest to understand the physics in one channel; however its logical limitation is that it is not able to account for other variables' distribution in a full scale reactor, like flow, temperature and species distribution. For these reasons it has had a limited application thereafter. The remaining approach is called the volume averaging model, which takes into account the whole reactor model assuming that the monolith can be modeled as a porous medium, i.e., the individual channels effect on the flow is only considered on an average basis and they are not modeled individually, which is a necessary assumption to perform this kind of simulations with current computers. This approach has been applied in many different investigations and the literature on this topic is quite extensive, therefore only the most relevant are reviewed.

As mentioned in the first paragraph, this chapter is focused mainly in the simulation without reactions, and therefore the literature survey is focused in this aspect. One of the earliest studies is [20], who performed a transient operation of monolithic catalytic converters by a two-dimensional volume average model to investigate the effect on flow and temperature distribution on the reactor performance using a Finite Element Analysis approach. This work was one of the first to look at the flow mal-distribution and its effect

on CO light-off. Some of their findings are that not only flow non-uniformities should be taken into consideration when studying the performance of this kind of reactor. It should also be considered some other physical parameters, as the he thermal mass of the reactor, exhaust gas temperature and stoichiometry, catalyst loading and gas-solid contact area. No attempt was mentioned to validate the simulations against experimental results, and only few elements were used due to computational limitations.

The inclusion of energy and mass balance equations followed the simulation of cold flow. An early work [21] developed a 3D model for a monolith and performed an extensive validation against experimental results. Temperature was included. The geometry was not that of a typical catalytic converter, however. A temperature distribution study is [22], who performed the simulation of the heat-up of the automotive catalyst during the cold-start and analyzed temperature distribution along the catalyst. However, they did not solve for the flow field.

Lai et al. [23] performed a three-dimensional non-reacting flow field simulation on a dual-monolith automotive catalytic converter under different operating conditions and geometries, which where compared against experimental values. Their findings showed that flow mal-distribution in the monolith depends on the inlet flow Reynolds number, the monolith flow resistance, and the inlet pipe length and its bending angles.

The use of CFD to study flow tailoring devices was also reported during the latter part of the 1990s. These studies were primarily cold flow 2D simulations [24, 25]. Shuai et al. [26] used 2D CFD to study the flow distribution in different converter configurations. They used three cone angles with a flow distribution device, and validated the results against experiments, although the agreement was not perfect. Tsinoglou et al. [27] studied transient flow distributions in the catalytic converter. The primary focus of that work was the development of a faster solution methodology than the traditional CFD approach.

Guojiang et al. [28] used CFX to study the influence of the flow distribution on the light-off performance. They employed the k-ε turbulence model. They compared the effect of a flow device on the light-off. The mass and heat transfer correlations used were not the ones now accepted as being generally valid. It is not clear that the thermal conductivities for the solid monolith are adjusted for the fluid phase and, finally, the results were not validated against experiments.

Other modeling methodologies exist, although they have not been popular mostly due to lack of enough validation or due to the computational resources required. One example

of this is [5], who modeled the catalytic converter by using the Lattice Boltzmann Method without reactions. Finally, two other methodologies exist to account the effects of the channels. One of them, called the representative channel method [29] consists in modeling the channels in detail, and then combining them with a macro-model for the whole converter. Because of the expense involved, usually only a few channels are modeled and an interpolation is made to estimate values between them. Another methodology for flow modeling was presented by Ozhan et al. [30], who used the open source Gerris software, which is based on the finite volume method, to perform a multi-scale model of a catalytic converter using an Adaptive Mesh Refinement technique and using an optimized way of computing the mesh adaption, with the aim to simplify the DNS approach of a catalytic converter flow modeling, and therefore no turbulence equations were used. In this work no reactions were included.

In the literature, there is no generally accepted flow modeling approach of catalytic converters. For example, [31] modeled the catalytic converter using three different turbulence models, k Quadratic High Reynolds, k High Reynolds and the v2f model, comparing against experimental results from particle image velocimetry (PIV) and it was shown that the modeling results disagree with the experimental results.

Finally, on another recent study, [17], the flow distribution study was performed using the single channel approach and the porous medium approach on a representative catalytic converter, using a 2D approach and comparing with the results obtained by PIV down-stream of the monolith. It was found that the different approaches produce relatively close peak velocities and velocity pro les and therefore the porous medium approach is a good compromise for the significant reduction in computational resources required.

This chapter is organized as follows: first a validation study with respect to data available in the literature is performed, to determine the model's accuracy. Once this is done, a parametric study of the different dimensions of the catalytic reactor is performed, to understand its effect on back-pressure and heat distribution.

3.2 Problem definition

3.2.1 Validation

The first step, prior going further in the problem of interest, was to validate a model against experimental data. [32] was chosen to do so. They used Laser Doppler

Anemometry (LDA) to evaluate the outlet flow distribution from a 400 Cells per Square Inch (CPSI) ceramic monolith, with a wall thickness of 0.165 mm and a diameter of 11.7 cm. The monolith was connected to a 4.92 cm diameter inlet pipe via a di user 7 cm in length.

For the experiment shown in Figure 5 of the reference, the average inlet velocity to the pipe was calculated to be 14 m/s. This number was determined by a numerical integration of the data points shown in their figure, and corresponds to a Reynolds number of about 43,000 in the inlet pipe. Assuming a channel size of 1.1 mm, and a monolith porosity,ϕ, of 0.75, the channel Reynolds corresponding to uniform flow in the channels was about 228. The axial permeability was computed using a Poiseuille flow assumption in square channels, according to [33]:

$$K = \frac{\phi D_H^2}{28.4} \tag{3.1}$$

Holmgren et al. [32] reported that they did not achieve a good match with experiments unless allowance was made for a weld at the join of the inlet pipe to the di user. Their weld was also modeled as a semi-circular domain protruding into the flow field, which is similar to what is inferred their approach was. Simulations were performed with and without the weld.

A variety of simulations were performed. Firstly, the monolith, diffuser and 7 cm of inlet pipe were simulated, with a uniform velocity pro le imposed at the inlet. Two finite element meshes were used. In the first the mesh was uniform, and in the second case a very ne mesh was used at the boundary layer along the walls. The first mesh used triangular elements and the second a mix of triangular and rectangular elements. A series of tests was performed to determine the mesh size required six levels of mesh size were used, whose number of elements and execution times can be found on Table 3.1. Sections of the mesh M4 are shown in 3.3, taken from the inlet of the di user. It is observed that the boundary layer mesh was required to give a reasonable velocity pro le. As the mesh becomes progressively finer, the solution converges to the same value. Meshes finer than M5 did not give any significant difference in the velocity pro le, and indeed the difference between the M4 and M5 is marginal. Further results are shown with the mesh size of M4.

Table 3.1: Details of meshes used to study the grid dependence

Designation	Elements	dof	Execution time, s
M1	1583	6460	18
M2	4570	17212	39
M3	8390	29626	60
M4	17800	62528	125
M5	39280	135101	320
M6	90300	288971	674

Figure 3.1 shows the predicted velocity pro le at a distance of 3 cm from the outlet of the monolith, which is the same physical location used for the LDA analysis made in [32]. The experimental points are shown as symbols, and the different lines show the simulated results with (a) the uniform mesh and no weld; (b) the boundary layer mesh and no weld and (c) the boundary layer mesh and a 2 mm diameter weld. In each of these cases the imposed inlet velocity pro le was uniform. It is clear that the simulation with the boundary layer mesh and the weld most closely approximates the solution, which agrees with the findings of [32]. Overall, based on the simulation results, it is concluded that the model is of sufficient accuracy to generate meaningful results, at least in the identification of realistic trends.

Figure 3.1 shows the predicted velocity pro le at a distance of 3 cm from the outlet of the monolith, which is the same physical location used for the LDA analysis made in [32]. The experimental points are shown as symbols, and the different lines show the simulated results with (a) the uniform mesh and no weld; (b) the boundary layer mesh and no weld and (c) the boundary layer mesh and a 2 mm diameter weld. In each of these cases the imposed inlet velocity pro le was uniform. It is clear that the simulation with the boundary layer mesh and the weld most closely approximates the solution, which agrees with the findings of [32]. Overall, based on the simulation results, it is concluded that the model is of sufficient accuracy to generate meaningful results, at least in the identification of realistic trends.

3.2.2 Geometry generation

For this study, a 2D axis-symmetric model was considered, showed in Figure 3.2. The geometry is composed of three zones. The inlet cone on the left, where the flow is coming

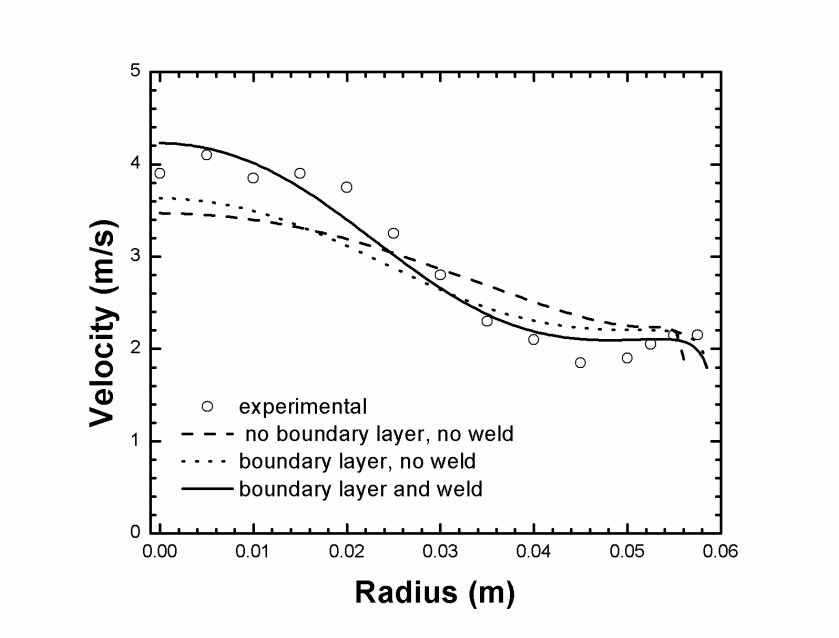

Figure 3.1: Velocity profile validation

into the converter, the monolith section in the center, where the reactions take place, and the outlet cone, which in this case is modeled symmetric with the inlet cone. The centerline shows where the axis is located.

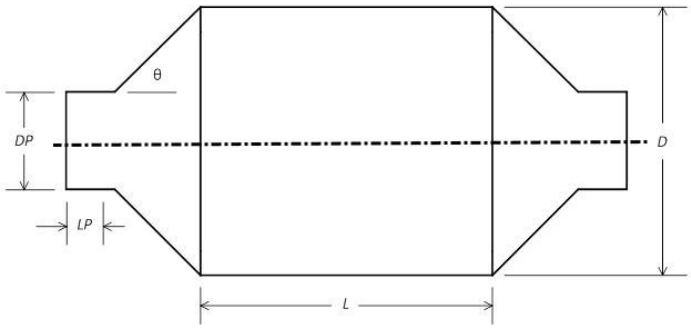

Figure 3.2: Diagram of the catalytic converter geometry studied with key lengths identified

The dimensions were chosen to represent a simple, although realistic catalytic converter. These dimensions can be found on table 3.2.

Table 3.2: Dimensions of the geometry

Parameter	Value	Description
DP	5.0 [cm]	Inlet pipe diameter
LP	5.0 [cm]	Inlet pipe length
D	13.5 [cm]	Monolith diameter
L	15.0 [cm]	Monolith length
	45	Cone angle

3.2.3 Mesh

Figure 3.3 shows a close up of the used mesh. An unstructured mesh was used with boundary layer elements and a total number of 39,280 elements.

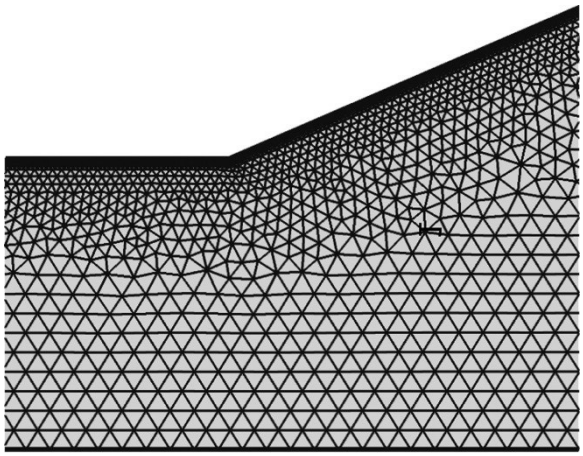

Figure 3.3: Cold flow mesh close-up from the inlet canning.

3.2.4 Physics

Governing equations

For modeling the gas phase in the inlet and outlet cone, in principle only the continuity equation 2.1 and momentum balance 2.3 is required. However the flow is known to be turbulent, and therefore this effect has to be taken into account. The chosen turbulence model was $k-\varepsilon$, because for comparison purposes it is the most suitable for this case due to its simplicity.

Boundary conditions

At the inlet different conditions were applied. In terms of gas space velocity (GHSV) it ranges from 25,000 h^{-1} to 100,000 h^{-1}. The former, referenced at 300 K gives and inlet

velocity of 7.6 [m/s] and corresponds to a Reynolds number of 24,000 in the inlet and justifies the use of a turbulence model. The turbulence intensity at the inlet is set to 5% and the turbulence length scale is set to 0.01 [m].

The canning walls are set to convective heat transfer with T_{inf} of 293 [K] and the heat transfer coefficient was set to 15 $\frac{W}{m^2K}$, whereas the monolith wall's convective heat transfer coefficient was set to 1.6 $\frac{W}{m^2K}$, representing a combined resistance of natural convection and conduction. The pressure at the outlet was set to 0 and outflow condition for the heat.

Table 3.3: Physical properties of the different monoliths studied

Property	A Standard	A2 Standard2	B thin wall	C Thin wall	D Ultrathin wall	E Ultrathin wall	F Ultrathin wall
Cells per square inch, CPSI	400	400	400	600	400	600	900
Cells per square meter, CPSM	620000	620000	620000	930000	620000	930000	1395000
Wall thickness, mil	7	6.5	4.3	4.3	2.5	3.5	2.5
Wall thickness, mm	0.1778	0.1651	0.1092	0.1092	0.0635	0.0889	0.0635
Substrate channel size, mm	1.092	1.105	1.161	0.928	1.207	0.948	0.783
Substrate volume fraction	0.260	0.243	0.165	0.200	0.097	0.164	0.144
Washcoat volume fraction	0.12	0.12	0.12	0.12	0.12	0.12	0.12
Fluid volume fraction (OFA)	0.620	0.637	0.715	0.680	0.783	0.716	0.736
Washcoat thickness, avg m	46.26	45.68	43.30	36.18	41.54	35.34	28.50
Hydraulic diameter, D_h, mm	1.000	1.1014	1.1074	0.855	1.123	0.877	0.726
Geometric surface area, GSA, $m^2=m^3$	2479	2514	2664	3182	2786	3264	4052
Bulk density substrate, $kg=m^3$	424.5	396.3	268.3	325.3	158.9	267.5	235.3
Bulk density nal, $kg=m^3$	556.5	528.3	400.3	457.3	290.9	399.5	367.3
Axial permeability, $10^8 m^2$	1.94	2.04	2.60	1.56	3.09	1.72	1.21
Axial thermal conductivity, solid	0.611	0.750	0.419	0.489	0.285	0.418	0.379
Radial thermal conductivity, solid	0.383	0.362	0.269	0.310	0.194	0.269	0.246

3.3 Results and discussion

3.3.1 Cold flow test

The next sets of graphs show the effects of various operating parameters on the flow distribution and pressure drop. To quantify the flow mal-distribution, a flow index was defined as the fraction of the mass flow that passes through the central core of the monolith, which is delineated by one half of the radius. This volume corresponds to one quarter of the total monolith volume, thus a flow index of 0.25 corresponds to a uniform flow distribution. Figures 3.4a and 3.4b show the effect of di user angle at three GHSV on the pressure drop and flow index for the standard monolith size, with a cell density of

400 CPSI and a 7 mil (0.007 inch) wall thickness (denoted as 400/7). Clearly, the overall pressure drop increases with velocity, which is expected. The pressure drop also increases with increasing di user angle, which effect is exacerbated at higher velocities. Furthermore, as the angle increases, more of the flow is directed through the central core of the monolith. The trend is similar for all inlet velocities tested. Over the last ten years, there has been considerable interest in using a variety of cell densities in catalytic converters to enhance the performance. Referring to Table 3.3 the variation of cell density and wall thickness affects many of the properties of the monolith. For example, higher cell density implies a lower cell hydraulic diameter, giving a lower permeability and a corresponding increase in pressure drop at a given velocity.

In the next series of simulations, the flow distribution under a set of cold flow conditions was used. All these simulations involved washcoated Cordierite monoliths, and were based on the properties of typical washcoated Cordierite monoliths shown in Table 3.3. Note that the permeability was computed using the hydraulic diameter and a constant of 32 (rather than 28.4) in Equation 3.1, because after washcoating the channel shape is nearer to circular than square [34]. All of the monoliths used were assumed to contain 12% by volume of washcoat, which is a typical value [34]. The base case monolith was 15 cm long (L) and 13.51 cm in diameter (D), which gives an L/D ratio of 1.11. For simulations where the L/D ratio was changed, the total monolith volume was held constant. The inlet and outlet pipes were both 5 cm in diameter and 2.5 cm long. The di user length was adjusted to give the required angle and the inlet and outlet diffusers had the same length and angle. The inlet velocity pro le to the pipe was uniform. An average inlet velocity of 7.6 m/s gave a gas hourly space velocity (GHSV) of 25 000 h^{-1}, referenced at 300 K. This velocity corresponds to an inlet pipe Reynolds number of about 24,000. The Reynolds number in the channel is of the order of 110. The latter number varies depending on the flow distribution in the channels.

Figures 3.5a and 3.5b show the effect of L/D ratio on pressure drop and flow index for the 400/7 monolith with a 40 degree di user angle. As the L/D ratio increases (the monolith gets longer), an increase in pressure drop was found. This effect occurs because the channel velocity increases as the L/D increases. The flow index drops as the monolith diameter decrease

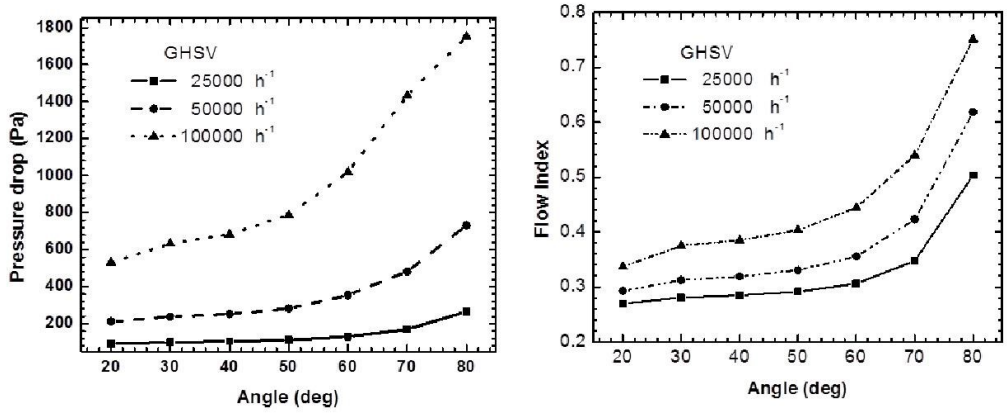

(a) (b)

(a) Pressure drop as a function of di user angle at (b) Flow index as a function of di user angle at different GHSV. The monolith was a 400/7 with different GHSV. The monolith was a 400/7 with an L/D of 1.11 and L/D of 1.11.

Figure 3.4: Angle study: Pressure drop and flow index as a function of the cone angle

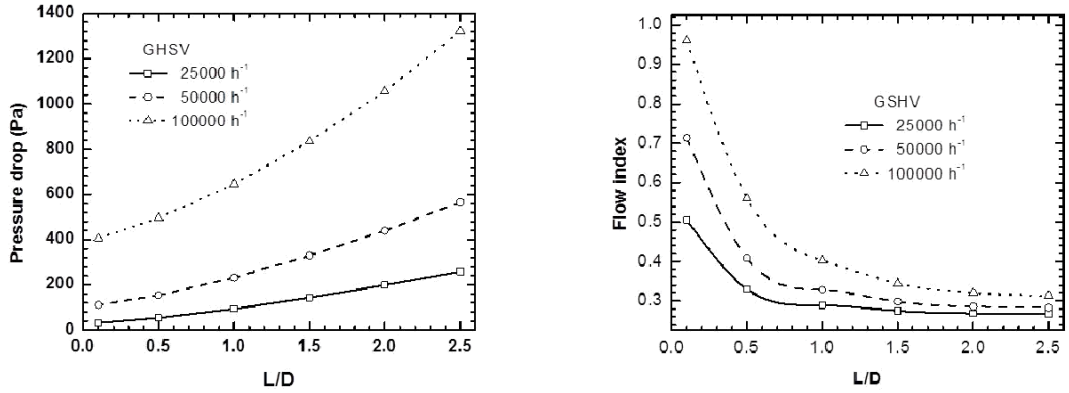

(a) (b)

(a) Pressure drop as a function of L/D ratio at (b) Flow index as a function of L/D ratio at different GHSV. The monolith was a 400/7 with different GHSV. The monolith was a 400/7 with a diffuser angle of 40 deg.

Figure 3.5: Aspect ratio study: Pressure drop and flow index as a function of the L/D ratio

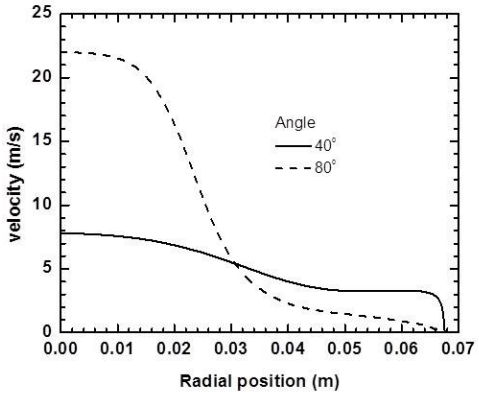

Figure 3.6: Velocity pro le at the outlet of the monolith for two different di user angles. The monolith was a 400/7 with an L/D ratio of 1.11.

Finally, the radial velocity profile is shown in Figure 3.6 at two diffuser angles for the 400/7 monolith with an L/D ratio of 1.11 at a GHSV of 25 000 h^{-1}. It has previously seen that the flow index is higher for a larger diffuser angle, and this figure shows the magnitude of the velocity differences.

3.3.2 Temperature ramp study

Following the cold flow tests, a series of simulations was performed in which the inlet temperature was ramped in the absence of chemical reaction. The ramp was 20 K/s. All simulations were performed at a GHSV of 25 000 h^{-1} referenced at 300 K (inlet velocity at 300 K of 7.6 m/s) with an L/D ratio was 1.11. The inlet velocity was increased as a function of temperature to maintain a constant inlet mass flow rate. The temperature was ramped from 300 K to 700 K over 20 s, and then held constant at 700 K until steady state was reached. The inlet velocity pro le was uniform. The fluid temperature was imposed at the inlet. The pipe and di user walls had convective boundary conditions, with an external temperature of 300 K and an overall heat transfer coefficient of 14.9 W/(m2K), which combined the resistances owing to natural convection and the 3 mm thick steel walls of the can. The body of the monolith has an overall heat transfer coefficient of 1.5 W/(m2K), which combined the effects of natural convection with a 3 mm thick insulation layer of thermal conductivity 0.2 W/(mK) and the walls of the steel can. The results are presented in terms of the flow index defined previously, and a temperature index. The temperature index is defined as the thermal energy contained within the central volume fraction equal to 0.25 compared to the overall energy within the monolith, and is in effect a ratio of the average temperature in the core divided by the average temperature in the entire monolith. Figure 3.7 shows the flow and temperature

indices for a di user angle of 40 as a function of time. Both indices show a transient behavior as the monolith heats. The flow index initially increases, then decreases before leveling out at a constant value. The temperature index shows a rise and fall also, before becoming constant. This is indicative of the monolith heating more rapidly in the central part, and then achieving a much more uniform temperature profile. The trends for all of the monolith types are the same.

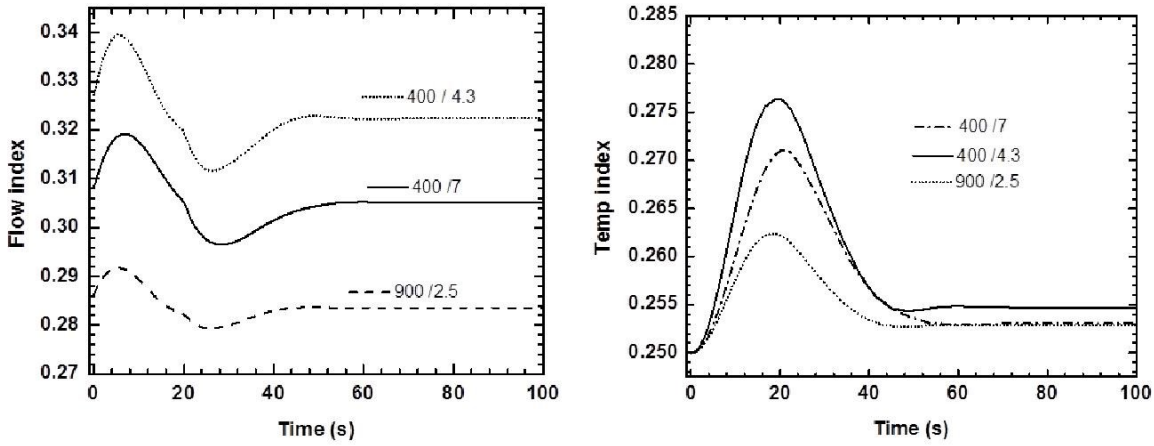

(a) (b)

(a) Flow index as a function of time for different (b) Temperature index as a function of time for monoliths at a GHSV of 25 000 h-1. The diffuser different monoliths at a GHSV of 25 000 h-1. The angle was 40 and the L/D was 1.11. diffuser angle was 40 and the L/D was 1.11.

Figure 3.7: Transient study: Flow index and Temperature index results

3.4 Chapter remarks

In this chapter a series of simulations for the full catalytic converter was performed using a continuum model. The effect of the different geometrical aspects of the converter, as well as the physical parameters of the monoliths was shown in terms of flow and temperature distribution. With the assumptions made in this work, the execution times are reasonable on a typical low cost PC with available commercial software. It was shown from the literature review that no approach is generally valid to model the flow field of this kind of converters. As shown in the literature survey [17], the porous medium approach provides good results when compared against the single channels simulations. However, it is mentioned that in terms of turbulence modeling, no consensus exists and therefore in this work a modeling error is implied due to this.

Considering the results obtained here, it is clear that the monolith substrate configuration has a significant impact on the flow and temperature distributions, and on the resulting

chemical reactions. Pressure drop is also a strong function of the substrate configuration. By altering and customizing the permeability distribution, it should be possible to achieve many desirable flow patterns, although the practicality of such designs would have to be carefully considered.

Chapter 4

4 Multi-scale modeling

4.1 Introduction

The main motivation of this chapter is to develop a detailed model of a catalytic converter to study the effect of the many configurations available, which have an impact on the flow and temperature patterns, as shown without reactions in the previous chapter. More precisely, in this chapter the study of the effect of wall thickness and cell density is performed, accounting for a complex mechanism reaction scheme and for washcoat diffusion. For making a fair comparison, all cases have the same catalyst loading, which means that the washcoat fraction is the same in all cases under study. To perform this kind of modeling, in this section two more degrees of complexity have to be added into the catalytic converter model studied in the previous chapter. Firstly, a complex reaction mechanism with several steps and species are considered. For this case, as an example of the methodology, the methane oxidation on a platinum catalyst was implemented, using the mechanism presented in [35]. The second degree of complexity is the inclusion of the washcoat diffusion effect, which has an important role on the mass transfer limitations, and therefore in the observed reaction rate. The strategy to solve for this complex problem is by using the lookup table technology and is based on [2]. Some more details on this are provided later on in this chapter, although for an in depth explanation it is suggested to see the reference.

The modeling of catalytic converters using complex mechanisms has been by itself challenging until recent times, mostly because of the computational resources required. For this reason, many of the earliest studies included only global kinetics, as for example [20]. After the mid-1990s more papers began to appear that included chemical reactions. Martin et al. [36] used a simplified zonal analysis for the flow and showed that flow mal-distribution could affect the light-off characteristics. Jeong and Kim [37, 38] used a 3D

analysis in a simulation study to show the influence of a warm-up catalyst on the light-off performance of a three way catalyst.

During the 2000s there were several papers that have included the reactions, usually using global kinetics without accounting for washcoat diffusion. This is usual considered a computational necessity. Indeed, one of the big challenges facing the converter modeler is the inclusion of realistic reaction chemistry [39]. Chakravarthy et al. [40] used an algebraic turbulence model for a single converter geometry in two dimensions, and included temperature and reaction. They validated their results using the experiments of Holmgren et al. [32], who have presented a clear set of experimental data. The trend in their results showed acceptable agreement with the experiments. The reactions were modelled using the representative channel approach. They apparently used the Voltz [41] model for CO and C3H6 oxidation, and did not include washcoat diffusion. Papers by Windmann et al. [42] and Campbell et al. [43] showed the effect of flow distribution on the light-off of a three way converter. Shuai and Wang [44] simulated temperature fields within a catalytic converter using simplified Voltz model kinetics. The simulations were 2D and were not validated against experiments. A single geometry was used, although the cone angle at the inlet was altered.

So far it has not been feasible to use a full scale model without making simplifications that may lead to a big loss of accuracy. Few of the reactor models studied in the literature include realistic kinetics, because considering this makes the modeling too computationally demanding. Indeed, including realistic kinetics remains a large challenge. [39, 45, 46] Also, the diffusion in the washcoat must be considered properly. It is well known that the washcoat layer has a variable thickness around the perimeter of the channel, especially in square channels [34], and that this non-uniform shape affects the values of the e effectiveness factors for the chemical reactions. [6,47,48]

A key variable of interest is the so-called light-off or ignition point, where 50 % of the inlet emissions are converted. Because much of the emissions occur during the cold-start, this variable is of keen interest. For example, Yamamoto et al. [49] studied the effect of wall thickness on the light-off performance of several 400 CPSI substrates, and demonstrated a reduction in light-off temperature of up to 20 K as wall thickness declined from 6 to 4 mil. The lower light-off temperature was attributed to the monolith thermal mass, which is smaller for thinner walls. This reduction can only affect the cold start performance, because the thermal mass is not important at steady state operation.

Others [50,51] have shown lower emissions at various stages of the drive cycle, which they attributed to an increase in geometric surface area of the substrate. The majority of these studies are experimental [52-55], although some modelling studies exist. [56-58]

On another study, [28] the influence of flow distribution on light-off performance was studied. They used CFX (finite volume) to model a single converter with and without a flow distribution device. The mass and heat transfer correlations used were not the ones now accepted as being generally valid. They also did not consider diffusion in the washcoat. It is not clear that the thermal conductivities for the solid monolith are adjusted for the fluid phase and, finally, the results were not validated against experiments.

More recently, [58] performed CFD simulations using AVL on monoliths of constant cell density with varying wall thickness. They compared their CFD results with the experimental velocity profile of [32]. They used Voltz [41] kinetics and ignored washcoat diffusion. It appears that the comparisons for different wall thickness did not use the same mass of washcoat in each case. A single converter geometry was tested. Liu [6] used FLUENT with a novel two zone method to model methane ignition in a ten liter volume reverse flow reactor. They validated their results with experiments.

The modeling of the catalytic converter is an exercise in multi-scale modeling; where the scales range from the nanometre to centimetre, and as shown in the previous paragraphs of this section, it is usual make assumptions for the washcoat diffusion when modeling the catalytic converter. The solution to the scale problem can be found by the development of a series of sub-models for the smaller scale processes that can then be incorporated into the large scale model. For example, one could solve a diffusion-reaction problem for the washcoat at each computational node in the system, to compute effective local reaction rates. However, inclusion of such sub-models in the classical manner leads to unrealistically large solution times, and therefore new methodologies must be developed.

Recent publications in the area of multi-scale model reduction demonstrate a feasible solution to this problem. The underlying methodology is to pre-compute solutions for the sub-models and to store the results in a lookup table, that is accessed during solution. [59-62] Depending on the level of complexity, the look-up table may be expensive to build, but once built is easy to use. The use of pre-computed rate data for complex reacting flows has been used for gas phase kinetics, and recently in single channel

monolith systems for complex kinetics, [63] as well as cases of complex washcoat design and reactor analysis [64-66] Nien et al. [2] very recently presented a detailed methodology for the systematic multi-scale model reduction in the context of catalytic converters. They demonstrated that all microscopic detail could be retained in a full scale converter model without significant loss in accuracy, with a huge saving in computer time.

This chapter is organized as follows: Firstly the problem details are presented, then the geometrical model is described. Later the physics are discussed and the geometrical discretization is presented. After presenting the background, two different studies are performed. First, a steady state execution was performed, to understand the effect of the different monoliths configurations under the steady state conditions. Afterwards, a transient study is performed, to simulate the cold start of the monolith. Different temperature ramps are used and the emissions and light-off curves are presented.

Then the difference of performances of the different configurations is understood as the sum of three effects, namely: Flow distribution, related to the monolith permeability (K), thermal effects, related to the monolith's thermal properties and finally the washcoat effects. For this, three more studies were performed, keeping constant the thermal mass, the permeability and the thermal conductivity. Finally, the effect of perturbations on the mass flow rate and in the temperature where computed, to get a better understanding of the changes in the inlet conditions. In all cases the total emissions are computed and the results are discussed.

Finally, it is worthwhile mentioning that part of the work presented in this chapter has been already published [67]. Also, in this work all the simulations that involve a reaction, get the source rate computed from the look-up tables and were built by Nien, published in [2].

4.2 Model overview

To understand the effects of parameters such as the monolith cell density and the wall thickness, it is necessary to describe the transport dynamics in these catalytic reactors. The channels of the honeycomb monoliths are of the order of 1 mm in size, therefore, notwithstanding the high fluid velocity (of the order of 1 to 10 m/s); the flow down the

channels is in the laminar region. The chemical reactions occur in the porous catalytic washcoat on the walls of the channel. The entry region of the channels is fairly short, and therefore most of the flow occurs in the fully developed region. The heat and mass transfer processes therefore play a large role in the reactor performance. The reactants must first di use from the gas phase to the gas/solid interface; thence they diffuse and react within the washcoat. The external mass transfer coefficients are independent of velocity, and are governed by molecular diffusion. In the washcoat, Knudsen diffusion plays the dominant role. From a geometrical standpoint, altering the wall thickness at constant cell density changes the channel size. If the amount of washcoat in the channel remains the same, then the thickness of the washcoat will alter. If the cell density is increased, then the channel diameter decreases. If the total washcoat loading in the whole monolith is preserved, this change will result in less washcoat per channel, which nominally translates into a thinner washcoat on average. Overall, a reduction in the channel size causes a decrease in the external heat and mass transfer resistance, whilst a reduction in the washcoat thickness gives a decrease in the internal mass transfer resistance. An increase in the cell density also gives an increase in the interfacial contact area between the fluid and the washcoat. A reduction in mass and heat transfer resistance usually improves performance. However, if the channel diameter is decreased, the pressure drop across the converter increases, which gives lower performance and a decrease in fuel economy. A change in pressure drop across the monolith substrate also influences the velocity distribution inside the converter, as shown in the previous chapter. The other main effect of changing the cell density and wall thickness is the effect on the thermal mass, as noted earlier. The thermal mass is an important parameter in start-up. The cell density and wall thickness also affect the monolith porosity. If the monolith porosity increases, then, assuming a constant mass flow rate, the mean residence time of the gas in the monolith will increase, resulting in a lower pressure drop and more time for reactions to occur.

To demonstrate the significance of the cell density effects, and to illustrate the multi-scale model reduction technique, methane oxidation was used. The multi-step mechanistic reaction scheme proposed by Deutschmann [35] was used. This system was adopted by Nien et al. [2] using the Cantera [68] kit in their investigation. The model contains 11 surface species and 23 surface reactions, and in Cantera another reaction is included for stability reasons with parameters that do not affect the final result. The mechanism is shown on table 4.2.

4.2.1 Geometrical model

A single geometrical configuration was used in this work, as shown in Figure 4.1. It is a two dimensional axis-symmetric model. It consists of an inlet pipe of diameter DP, a di user cone of angle, and a porous zone (monolith) of length L. The monolith is insulated with a layer 0.005 m thick, to give a total reactor diameter D. Downstream, the outlet di user cone has the same angle and length as the inlet cone. The outlet pipe was the same length and diameter as the inlet pipe. All of the dimensions are given in Table 4.1. It should be emphasized here that the exact geometrical shape (e.g., di user cone angle and length, ratio of inlet and outlet pipe diameter to the monolith diameter, monolith shape, etc.) will all have an effect on the results. For example, the di user cone angle plays a role on the degree of flow separation and recirculation, which is in turn affected by the back pressure which is altered by the cell density. Therefore, to determine the best configuration for any vehicle requires a detailed exercise in shape optimization for all geometrical parameters. In this work, the changes are limited to the cell density and wall thickness.

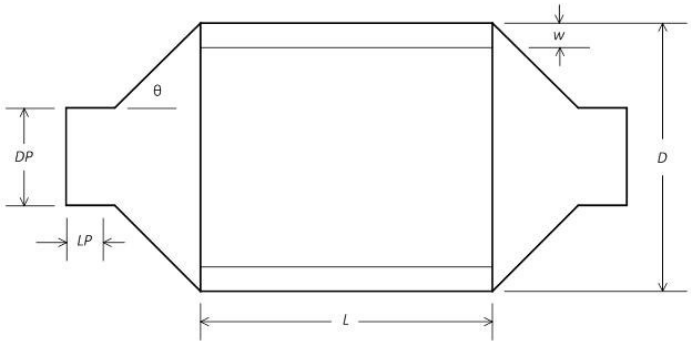

Figure 4.1: Diagram of the catalytic converter geometry studied with key lengths identified.

Six combinations of cell density and/or wall thickness were used, with values selected based on ceramic monolith substrates with square channels available from Corning. All monoliths were assumed to have 12 % by volume washcoat present, which formed fillets in the corners. The physical parameters of the six monoliths are given in Table 3.3. The insulation used had a thermal conductivity of 0.04 W/(mK), a density of 25 kg/m3 and a heat capacity of 670 J/(kgK). The fillet shape that is developed in each corner is illustrated in Figure 2, which shows scale drawings of one eighth of the washcoat cross section in each channel. The average reaction rate in the different washcoats must be correctly accounted for in the comparison.

Table 4.1: Dimensions of the geometry

Parameter	Value	Description
DP	5 [cm]	Inlet pipe diameter
LP	5.0 [cm]	Inlet pipe length
D	13.5 [cm]	Monolith diameter
L	16.3 [cm]	Monolith length
wi	0.5 [cm]	Insulation thickness
Angle	40	Cone angle

4.2.2 Mesh

The meshing of the aforementioned geometry is shown in Figure 4.2 has a structured mesh in the monolith part to reduce artificial diffusion produced by an unstructured mesh, because it is known that in the channels there is no axial flow, and therefore an unstructured mesh can include artificial diffusion. A boundary layer in the canning has been included, and it has been considered that the y+ value is above 11.06 to ensure the proper use of the wall functions.

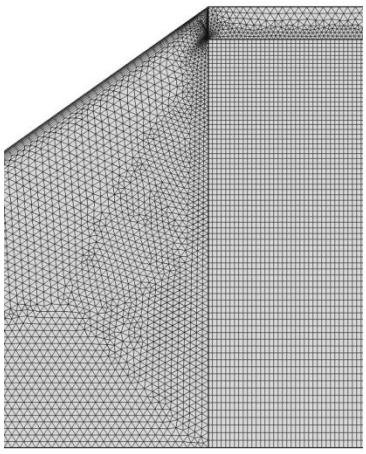

Figure 4.2: Model mesh of the geometry

A mesh study was performed with cold flow, measuring the axial velocity at the center-line in the front part of the monolith. The results can be found on Figure 4.3. It was found that 30,000 elements where enough to model properly the flow field because no significant change was found after increasing the number of elements.

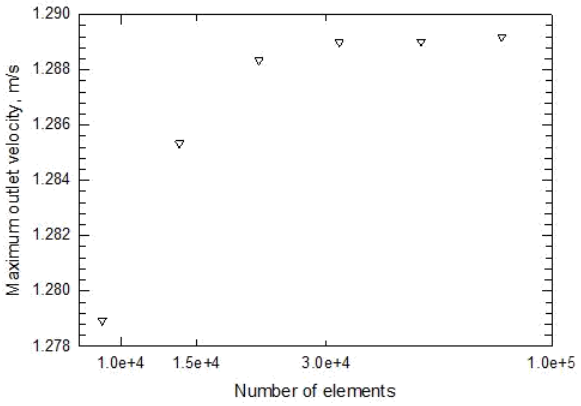

Figure 4.3: Mesh independence study

4.2.3 Physics

The physical properties of the different types of monolith are the same as shown on table 3.3. The only difference is that in this case the selected standard case is the 6.5 mil, called A2. Since the cell densities and the wall thickness vary, but keeping constant the amount of washcoat for each case of 12%, the washcoat shapes have to be different for each case, which has an implication on the mass transfer for each case. From the work of Nien et al. [2] the different shapes of the washcoat fillets are shown in Figure 4.4, where one octant of the geometry is shown and it is assumed that for every case the final shape is circular on a square channel.

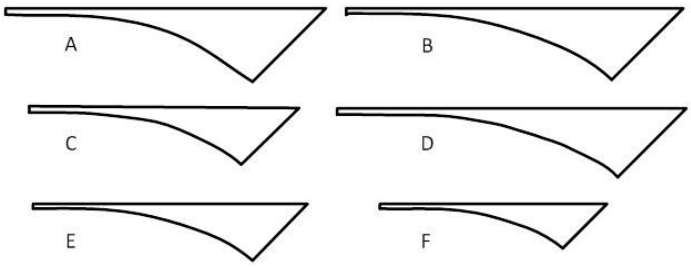

Figure 4.4: Fillets for the different types of cell densities [2]

The enthalpy change of reaction is taken from [1] as follows:

$$\Delta H_R = -8.025\ 10^5 + 1.587 \cdot T + 8.48\ 10^{-3} \cdot T^2 - 4.087\ 10^{-6} \cdot T^3 + 2.163\ 10^{-9} T^3 \qquad (4.1)$$

Boundary conditions

For the flow boundary conditions, at the inlet to the system the velocity is specified. The inlet velocity was adjusted with changing temperature to maintain a constant mass flow rate. Dirichlet boundary conditions of specified temperature and species concentration were imposed. At the reactor outlet, pressure outlet boundary conditions were used for the flow. The temperature boundary conditions imposed were convection conditions at the outside surface of the reactor. An imposed value of the heat transfer coefficient and surrounding temperature was used. For the heat transfer coefficient, a value of 15 W/(m2K) was used, which is typical for natural convection. The surrounding temperature was 293 K. Zero flux conditions were imposed for the mass conservation equations at the external surfaces.

Table 4.2: Kinetic parameters of the ammonia oxidation, taken from [35]

								A	E_a	S^0
R1	H_2	+	$2Pt_{(s)}$	$\rightarrow$	$2H_{(s)}$					0.046
R2	$2H_{(s)}$	$\rightarrow$	H_2	+	$2Pt_{(s)}$			$3.7{\cdot}10^{21}$	67.4-6.0 $\theta_{H_{(s)}}$	
R3	H	+	$Pt_{(s)}$	$\rightarrow$	$2H_{(s)}$					1.00
R4	O_2	+	$2Pt_{(s)}$	$\rightarrow$	$2O_{(s)}$					0.07
R5	$2O_{(s)}$	$\rightarrow$	O_2	+	$2Pt_{(s)}$			$3.7{\cdot}10^{21}$	213.2-60 $\theta_{O_{(s)}}$	
R6	O	+	$Pt_{(s)}$	$\rightarrow$	O(s)					1.00
R7	H_2O	+	$Pt_{(s)}$	$\rightarrow$	$H_2O_{(s)}$					0.75
R8	$H_2O_{(s)}$	$\rightarrow$	H_2O	+	$H_2O_{(s)}$			$1.0{\cdot}10^{13}$	40.3	
R9	OH	+	$Pt_{(s)}$	$\rightarrow$	$OH_{(s)}$					1.00
R10	$OH_{(s)}$	$\rightarrow$	$Pt_{(s)}$	$\rightarrow$	$OH_{(s)}$			$1.0{\cdot}10^{13}$	192.8	
R11	$H_{(s)}$	+	$O_{(s)}$	$\rightleftharpoons$	$OH_{(s)}$	+	$Pt_{(s)}$	$3.7{\cdot}10^{21}$	11.5	
R12	$H_{(s)}$	+	$O_{(s)}$	$\rightleftharpoons$	$H_2O_{(s)}$	+	$Pt_{(s)}$	$3.7{\cdot}10^{21}$	17.4	
R13	$OH_{(s)}$	+	$OH_{(s)}$	$\rightleftharpoons$	$H_2O_{(s)}$	+	$O_{(s)}$	$3.7{\cdot}10^{21}$	48.2	
R14	CO	+	$Pt_{(s)}$	$\rightarrow$	$CO_{(s)}$					0.84
R15	$CO_{(s)}$	$\rightarrow$	CO	+	$Pt_{(s)}$			$1.0{\cdot}10^{13}$	125.5	
R16	$CO_{2(s)}$	$\rightarrow$	CO_2	+	$Pt_{(s)}$			$1.0{\cdot}10^{13}$	20.5	
R17	$CO_{(s)}$	+	O_2	$\rightarrow$	$CO_{2(s)}$	+	$Pt_{(s)}$	$3.7{\cdot}10^{13}$	105.0	
R18	CH_4	+	$2Pt_{(s)}$	$\rightarrow$	$CH_{3(s)}$	+	$H_{(s)}$			0.01
R19	$CH_{3(s)}$	+	$Pt_{(s)}$	$\rightarrow$	$CH_{2(s)}$	+	$H_{(s)}$	$3.7{\cdot}10^{21}$	20.0	
R20	$CH_{2(s)}$	+	$Pt_{(s)}$	$\rightarrow$	$CH_{(s)}$	+	$H_{(s)}$	$3.7{\cdot}10^{21}$	20.0	
R21	$CH_{(s)}$	+	$Pt_{(s)}$	$\rightarrow$	$C_{(s)}$	+	$H_{(s)}$	$3.7{\cdot}10^{21}$	20.0	
R22	$C_{(s)}$	+	$O_{(s)}$	$\rightarrow$	$CO_{(s)}$	+	$Pt_{(s)}$	$3.7{\cdot}10^{21}$	62.8	
R23	$CO_{(s)}$	+	$Pt_{(s)}$	$\rightarrow$	$C_{(s)}$	+	$O_{(s)}$	$1.0{\cdot}10^{18}$	184.0	

Regarding the species, at the inlet the mass fractions are as follows, in mass fractions:

CH_4: 0.1%, O_2: 6%, H_2O: 6%, N_2: 87.9%

4.3 Results and discussion

4.3.1 Steady state study

The first study was to compare the light-off point when the simulations were performed at steady state. For doing so, several runs were performed with different inlet temperatures. The GHSV was set to 25,000 h^{-1} referenced at 300 K. The results can be found in Figure 4.5. It was found that below 775 K the difference between the different configurations is small. However, at higher inlet temperatures it was found that the 900/2.5 configuration presented the best performance in terms of conversion.

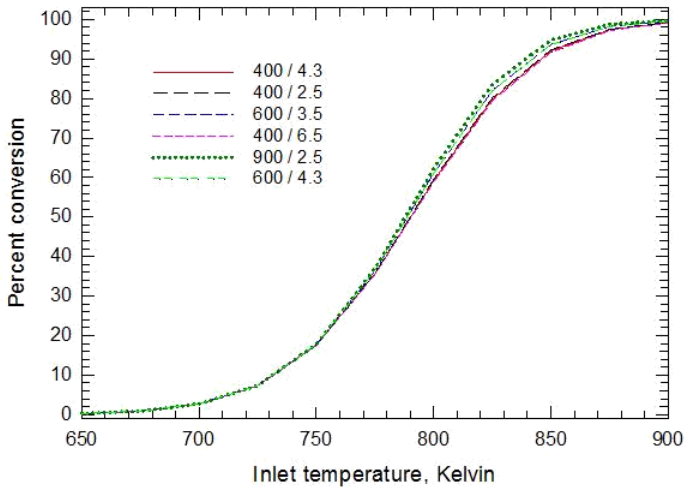

Figure 4.5: Conversion vs. inlet temperature for steady state simulations

On the opposite side, all the configurations with 400 CPSI showed the worse performance. This can be explained by the reduction of internal and external mass transfer resistance due to the higher cell density. Also, flow distribution may play a role in this case. As shown in the previous chapter, higher permeabilities produce a more uniform pro le. In this case the thermal mass of the different monoliths play no role because the simulations were performed at steady state. Taken together, monoliths F, E and C (600 and 900 CPSI) have the lowest diffusion (internal and external) mass

transfer resistance, whilst A, B and D (the three 400 CPSI cases) have the worst. The external resistance for D is greater than for A and B, however, the internal resistance is lower.

Summarizing, the results suggest that mass transfer resistance, either internal and external, play the most important role in this case and it is an interesting result, considering that many of the results presented in the literature do not consider diffusion in the washcoat or assumptions are made regarding this. On the other side, the differences found are visible only on a narrow temperature range, and also their magnitude is relatively small.

4.3.2 Transient study

The transient performance of catalytic converters is intuitively of paramount importance. In this case the thermal mass is also important, as it will affect the time required to reach operating temperature for cold start operation. The thermal mass also affects the cooling rate during cases of decreased engine load, or, for hybrid vehicles, the situation when the engine is not operated.

The first set of transient simulations performed was meant to simulate a cold start. For these experiments, the inlet temperature was initially set at 300 K, and the steady state solution obtained for a GHSV of 25,000h ^{1}. The inlet temperature was then ramped linearly at constant mass flow rate until a final inlet temperature of 950 K was attained, at which point the temperature was held constant and the simulation continued until steady state was achieved. Figure 4.6 shows methane conversion as a function of time for three inlet temperature ramp rates (a) 5 K/s, (b) 20 K/s and (c) 50 K/s.

Note that the order of increasing thermal mass (overall bulk density) is D, F, E, B, C, A. The performance of each converter can be compared by assessing the emissions over the cycle. Two calculations are presented. In the first, the results of which are shown in Table 4.4, the inlet temperature required to achieve a given conversion level is shown for the six geometries, for each of the three temperature ramps. It is noted that in all cases, monolith E (600/3.5) had the lowest inlet temperature for each of the given levels of fractional conversion of methane.

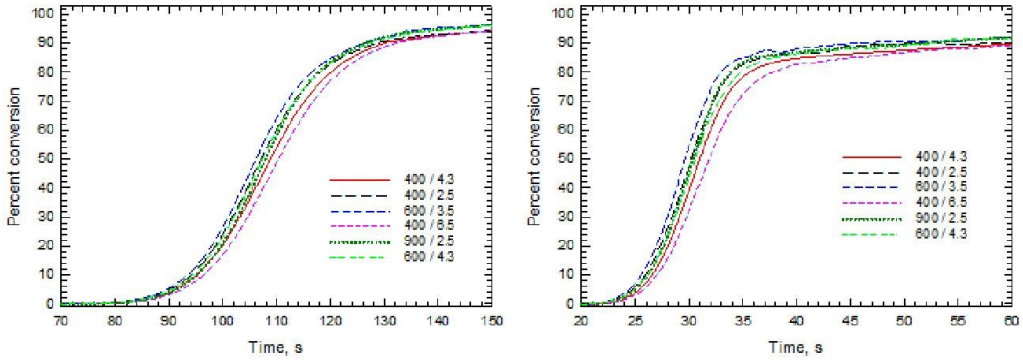

(a) 5 K/s (b) 20 K/s

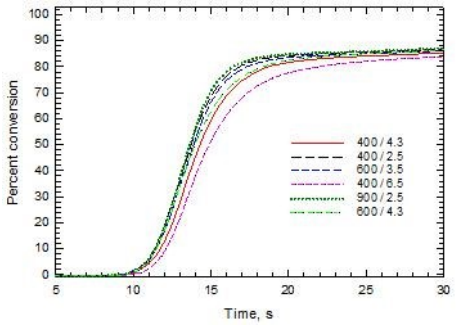

(c) 50 K/s

Figure 4.6: Methane conversion vs. time for different inlet temperature ramp rates.

This monolith does not have the lowest thermal mass. It was found that for the fastest ramp, the inlet temperature has reached the maximum value before even 25% conversion is achieved. It is thus perhaps more instructive to examine the cumulative emissions of methane produced over the entire warm-up period. The total emissions where computed by integrating the mass fraction of methane in the effluent over time, and multiplying by the total mass flow rate, shown in Equation 4.2:

$$m_{CH_4} = \dot{m} \int_{t_0}^{t_f} (1 - w_{CH_4}) dt \tag{4.2}$$

Table 4.3: Cumulative emissions, absolute and relative for the three temperature ramps. The relative emissions represent the percent reduction from the standard case, Monolith A.

	5 K/s		20 K/s		50 K/s	
	Emissions, g	Reduction	Emissions,g	reduction	Emissions,g	reduction
A 400/6.5	1.7848	0.00 %	0.6101	0.00 %	0.3691	0.00 %
B 400/4.3	1.7663	1.04 %	0.5973	2.10 %	0.3567	3.36 %
C 600/4.3	1.7250	3.35 %	0.5323	7.83 %	0.3271	11.38 %
D 400/2.5	1.7475	2.09 %	0.5842	4.25 %	0.3456	6.37 %
E 600/3.5	1.6765	6.07 %	0.5372	11.95 %	0.3313	10.24 %
F 900/2.5	1.7293	3.11 %	0.5523	9.47 %	0.3129	15.23 %

The results for these calculations are shown in Table 4.3. The total mass in grams of methane emitted is given, as is the percent reduction from the standard case, monolith A(400/6.5). It was observed that for the highest ramp rate, 50 K/s, the 900 CPSI monolith (F) has the lowest emissions, whilst for the other ramps the 600/3.5 monolith (E) was the best, which was consistent with the results shown in Table 4.4. Indeed, for these lower ramp rates, the 900 CPSI monolith was second or third in performance. Therefore, not only are the geometric properties of significance, but also the operating conditions.

Table 4.4: Inlet temperatures required to achieve 25, 50 and 75 % conversion for three inlet temperature ramps.

	Monolith type					
	A 400/6.5	B 400/4.3	C 600/4.3	D 400/2.5	E 600/3.5	F 900/2.5
	25 % conversion					
5 K/s	814.79	807.67	802.54	801.25	797.48	806.47
20 K/s	883.90	871.43	863.15	857.22	849.37	863.05
50 K/s	950.00	950.00	950.00	950.00	950.00	950.00
	50 % conversion					
5 K/s	851.46	843.79	836.61	835.56	830.59	839.52
20 K/s	936.95	919.31	911.34	903.32	891.63	907.22
50 K/s	950.00	950.00	950.00	950.00	950.00	950.00
	75 % conversion					
5 K/s	894.75	886.55	876.39	875.00	869.38	876.74
20 K/s	950.00	919.31	950.00	950.00	941.93	950.00
50 K/s	950.00	950.00	950.00	950.00	950.00	950.00

It was pointed out in the introduction that all of the geometrical parameters have effects on the results, and that is the reason to ensure that all of the effects are included in a

consistent way. Although with the real physical system one is forced to accept what is technically feasible, with computer simulation, it is possible to run scenarios to determine the effects of different parameters without the influence of the others. Taking the 20 K/s ramp, the simulations were run for the same monoliths but setting the bulk density to be same in all cases, at 428.8 kg/m3. The resulting light-off curves are shown in Figure 4.7, and the cumulative emissions in Table 4.5. The same cases were also run (constant thermal mass) where the axial permeability was held constant (which thus implies the same flow distribution), and then the case when the radial thermal conductivity was also held constant. The cumulative emissions for these latter two cases are also shown in Table 4.5, whilst the light-off curves are displayed in Figure 4.7. It was found that for these three scenarios, monolith F becomes the best performer. It can be concluded also that for these three properties, the thermal mass is the most influential, and also the one that can realistically be controlled independently.

Table 4.5: Cumulative emissions in g for a ramp rate of 20 K/s with different parameters held constant.

Configuration	Base case	Constant and thermal mass	Constant thermal mass and permeability	Constant thermal mass permeability and conductivity
A 400/6.5	0.6101	0.5964	0.5964	0.5964
B 400/4.3	0.5973	0.6025	0.6029	0.5994
C 600/4.3	0.5623	0.5608	0.5592	0.5579
D 400/2.5	0.5842	0.6085	0.6102	0.6020
E 600/3.5	0.5372	0.5769	0.5760	0.5735
F 900/2.5	0.5523	0.5577	0.5573	0.5549

Although the light-off behavior is of critical importance, the transient behavior resulting from changes in engine load (and hence exhaust gas temperature and mass flow rate) is also of interest. Two simulations were performed; in the first the temperature was reduced and then increased at constant mass flow rate; in the second both the temperature and mass flow rate were first reduced and then increased. The initial inlet temperature was 900 K with steady state. The inlet temperature was then varied over the time interval of 0 to 20 s using the function:

$$T_{in} = 700 \cdot \cosh(0.0739(t - 10)) \tag{4.3}$$

This function gives an inlet temperature of 900 K at 0 s, 700 K at 10 s, and finally 900 K at 20 s. The inlet temperature was then held at 900 K for a further 20 s. For a variation of

inlet mass flow rate, the inlet velocity was programmed to change according to the function:

$$v_{in} = 3.537 \cdot \cosh(0.01317(t - 10)) \tag{4.3}$$

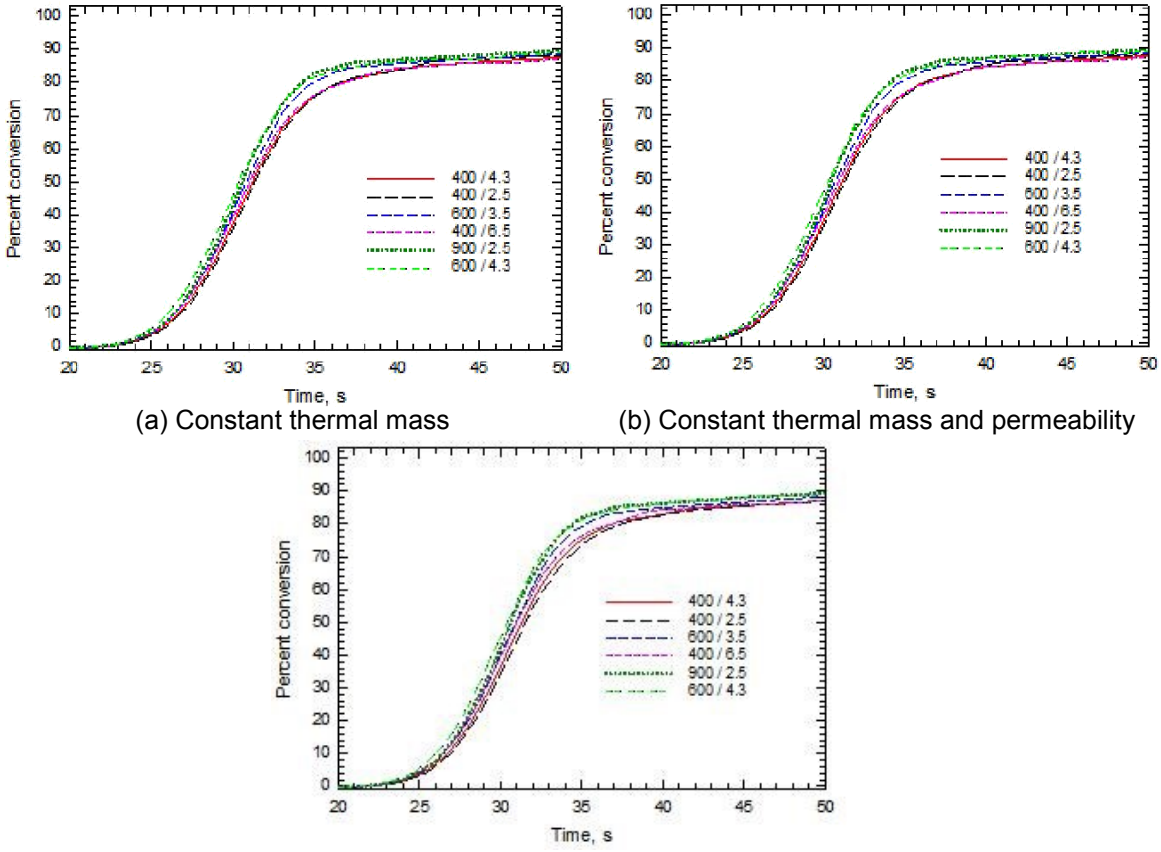

(a) Constant thermal mass

(b) Constant thermal mass and permeability

(c) Constant thermal mass, permeability and thermal conductivity

Figure 4.7: Transient methane conversion vs. time for inlet temperature ramp rate of 20 K/s

For times greater than 20 s the inlet velocity was held constant at 7.074 m/s. The conversion as a function of time for the two cases is shown in Figure 4.8, and the cumulative emissions are given in Table 4.6. It is seen that the monolith with the lowest thermal mass (D, 400/2.5) drops to the lowest temperature, and hence lowest conversion, in each case. For the case of the temperature change only, monoliths B, F and E, which have similar thermal masses, respond in a similar way, and finally the best performer was A, the monolith with the highest thermal mass. When both the inlet temperature and velocity changed, monolith D was by far the worst, with the others showing less difference. However, it can be seen that properties other than the thermal mass are significant.

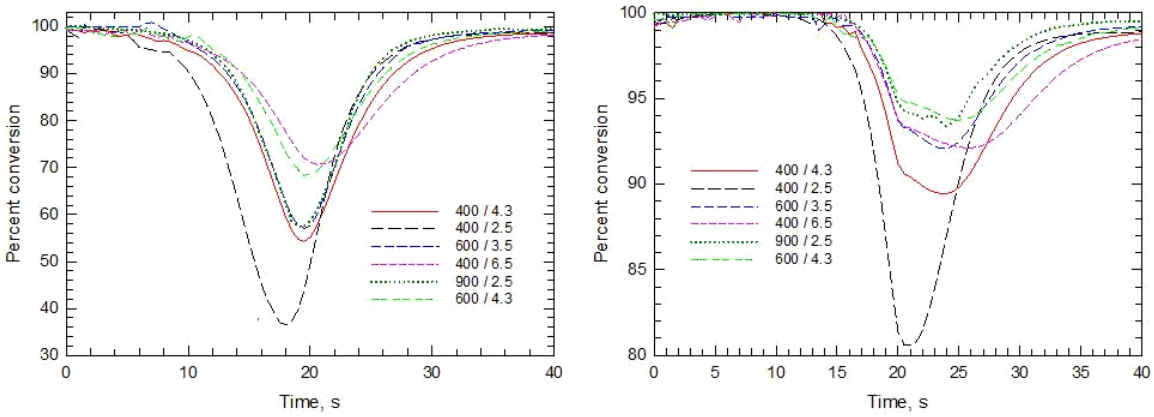

(a) (b)

(a) perturbation of the temperature at constant mass flow rate (b) perturbation of both temperature and mass flow rate

Figure 4.8: Transient conversion as a function of time

Table 4.6: Cumulative emissions in g for perturbations in inlet temperature only, and inlet temperature and mass flow rate

Configuration	Temperature perturbation	Temperature and mass perturbation
A 400/6.5	0.0587	0.0176
B 400/4.3	0.0732	0.0193
C 600/4.3	0.0520	0.0124
D 400/2.5	0.0962	0.0241
E 600/3.5	0.0607	0.0128
F 900/2.5	0.0579	0.0101

4.4 Chapter remarks

In this chapter the study of the effect of wall thickness and cell densities of catalytic converters including the washcoat diffusion and using a complex mechanism was performed. It has been shown that dependency of the performance of the reactor with respect to the cell density and wall thickness. There are many factors that are affected when the cell density is changed, and if a fair performance comparison is desired then all of the micro-scale detail must be included in a consistent manner. Taking advantage of the simulation approach, it was possible to separate the causes of the different

performances of the monoliths in three components: Flow distribution, thermal distribution and mass transfer contribution. This was performed by keeping constant some key variables which allow identifying the causes of the different performances according to the aforementioned classification. It has been found quantitatively that the major contribution to the different performance was due to the thermal mass. Another finding, in line with the previously mentioned, is that at steady state the differences of the light-off curves for the different cases are small, which also indicates that the heat effects are considerable. Finally, the effect of transient perturbations was examined: first changing only the temperature keeping the mass flow constant, and later adding a perturbation to the mass flow.

Another objective of this chapter was to demonstrate the ability of the look-up table approach to solve this type of full scale reactor problem. As it has been pointed out, to do a fair comparison of the performance of the monolith substrates requires the inclusion of the washcoat diffusion reaction sub-model. It is arguably arbitrary to make a comparison of execution times for different approaches, because the differences will depend on the problem definition and the specified operating conditions, as well as numerical factors such as mesh size, solution algorithm, required accuracy, etc.

Chapter 5

5 Summary and Conclusions

5.1 Contributions of this thesis

The main contribution of this thesis is the comprehensive comparison of different monolith configurations for automotive catalytic converters considering the cell densities and the wall thicknesses. A detailed study of the effect of the geometry on flow and temperature distribution and pressure drop was performed, which provides better understanding for design and later, with the inclusion of reactions, the effects of the different monolith configuration could be explored, using a complex Methane oxidation mechanism and considering the diffusion into the washcoat. It has been accounted for the amount of catalyst has to be employed in each case, so a fair comparison can be made. It has been presented a practical usage of the multi-scale model reduction, which is one of the hardest problems in automotive catalytic converters modeling, coupled with a complex kinetic mechanism performed on a commercially available computer requiring computational times that range from minutes to less than 10 hours depending on the study. This was done by using the look-up table technology, which was done by Nien and it is been already published [2].

5.2 Directions for future work

Further studies may include the effect of different turbulence models on the flow patterns, and finally in the overall performance of the catalytic converter. As mentioned in Chapter 3, this topic is still developing and it would be interesting to evaluate the consequence of using different turbulence models on the overall performance of the catalytic converter, and to see if this would make an effect on the monolith comparison performed in this work. Another direction for further work is to consider a 3D geometry, which includes asymmetries, and to study the effect on the reactor performance. Finally, the device studied in this work has been analyzed isolated from its system, and therefore it would be reasonable considering a more realistic model for the engine.

Bibliography

[1] R.Hayes and S. Kolaczkowski. *Introduction to catalytic combustion.* Gordon and Breach Science Publishers, 1997.

[2] T. Nien, J.P. Mmbaga, R.E. Hayes, and M. Votsmeier. Hierarchical multi-scale model reduction in the simulation of catalytic converters*. Chemical Engineering Science*, 23(1):362-375, 2013.

[3] E.N. Fuller, P.D. Schettler, and J.C. Giddings. New method for prediction of binary gas-phase diffusion coefficients. *Industrial and Engineering Chemistry*, 58(5):18-27, 1966.

[4] R. Aris. On the dispersion of a solute in a fluid owing through a tube. *Proceedings of the Royal Society A: Mathematical, Physical and Engineering Sciences*, Paper 2000-01-0207(235):67-77, 1956.

[5] F. Bertrand, C. Devals, D. Vidal, C. S. de Preval, and R. E. Hayes. Towards the simulation of the catalytic monolith converter using discrete channel-scale models. *Catalysis Today,* 188(1):80-86, 2012. Modeling of Exhaust-Gas After-Treatment.

[6] B. Liu, R.E. Hayes, Y. Yi, J. Mmbaga, M.D. Checkel, and M. Zheng. Three dimensional modelling of methane ignition in a reverse flow catalytic converter. *Computers and Chemical Engineering,* 31(4):292-306, 2007.

[7] R.E. Hayes, A. Rojas, and J. Mmbaga. The effective thermal conductivity of monolith honeycomb structures. *Catalysis Today*, 147, Supplement(0):S113-S119, 2009. 3rd International Conference on Structured Catalysts and Reactors, ICOSCAR-3, Ischia, Italy, 27-30 September 2009.

[8] O. Reynolds. An experimental investigation of the circumstances which determine whether the motion of water shall be direct or sinuous, and of the law of resistance in parallel channels. *Philosophical Transactions of the Royal Society of London*, 174:pp. 935-982, 1883.

[9] D.Wilcox. *Turbulence Modeling for CFD*. DCW Industries, 1994.

[10] O. Reynolds. On the dynamical theory of incompressible viscous fluids and the determination of the criterion. *Philosophical Transactions of the Royal Society of London. A*, 186:pp. 123-164, 1895.

[11] J. Boussinesq. Essai sur la theorie des eaux courantes*. Memoires presents par divers savants a l'Academie des Sciences*, 23(1):1-680, 1877.

[12] P. R. Spalart and S. R. Allmaras. A one-equation turbulence model for aerodynamic flows. *AIAA*, Paper 92-0439, 1992.

[13] W. Rodi. *Turbulence Models and Their Application in Hydraulics*. IAHR Monographs. Taylor & Francis, 1993.

[14] F. R. Menter. Two-equation eddy-viscosity turbulence models for engineering applications. *AIAA*, 32(8):1598-1605, 1994.

[15] R.E. Hayes, A. Fadic, J. Mmbaga, and A. Najafi . CFD modelling of the automotive catalytic converter. *Catalysis Today*, 188(1):94-105, 2012. Modeling of Exhaust-Gas After-Treatment.

[16] H. Abbasfard, M. Ghanbari, A. Ghasemi, G. Ghahraman, S. . Jokar, and M. R. Rahimpour. CFD modelling of flow mal-distribution in an industrial ammonia oxidation reactor: A case study. *Applied Thermal Engineering*, 67(12):223-229, 2014.

[17] S. Porter, A. Yamin, S. Aleksandrova, S. Benjamin, C.A. Roberts, and J. Saul. An assessment of cfd applied to steady flow in a planar diffuser upstream of an automotive catalyst. *SAE Technical Paper*, Paper 2014-01-2588, 2014.

[18] R.E. Hayes, S.T. Kolaczkowski, and W.J. Thomas. A finite element model for a catalytic monolith reactor. *Computers in Chemical Engineering,* 16(7):645-657, 1992.

[19] B. Liu, R.E. Hayes, Y. Yi, J. Mmbaga, M.D. Checkel, and M. Zheng. Modelling catalytic monoliths for automobile emission control. *Chemical reactor technology for environmentally safe reactors and products*, 31(4):547- 576, 2007.

[20] K. Zygourakis. Transient operation of monolith catalytic converters: a two-dimensional reactor model and the effects of radially nonuniform flow distributions. *Chemical Engineering Science*, 44(9):2075- 2086, 1989.

[21] R. Jahn, D. Snita, M. Kubicek, and M. Marek. 3-d modeling of monolith reactors. *Catalysis Today*, 38(1):39-46, 1997. Dynamics of Catalytic Systems '96 (Paper Presented at the 2nd International Symposium on the Dynamics of Catalytic Systems, Praque, August 1996).

[22] T. Kirchner and G. Eigenberger. On the dynamic behavior of automotive catalysts. *Catalysis Today*, 38(1):3-12, 1997. Dynamics of Catalytic Systems '96 (Paper Presented at the 2nd International Symposium on the Dynamics of Catalytic Systems, Praque, August 1996).

[23] M.-C. Lai, T. Lee, J.-Y. Kim, C.-Y. Cheng, P. Li, and G. Chui. Numerical and experimental characterizations of automotive catalytic converter internal flows. *Journal of Fluids and Structures*, 6(4):451-470, 1992.

[24] A. Heibel and M.A.A. Spaid. A new converter concept providing improved flow distribution and space utilization. *SAE Spring Fuels and Lubricants*, 60(2):SAE Paper No. 990768, 1999.

[25] J. Wollin and S.F. Benjamin. A study of the flow performance of ceramic contoured substrates for automotive exhaust catalyst systems. SAE Trans., J. Fuels Lubricants, 108(1):407-413, 1999.

[26] S. Shi-jin, W.Jian-xin, Z. Ren-jun, and C. Jun-rui. Study on flow characteristics of automotive catalytic converters with various configurations. *SAE Technical papers*, Paper 2000-01-0208, 2000.

[27] D.N. Tsinoglou, G.C. Koltsakis, D.K. Missirlis, and K.J. Yakinthos. Transient modelling of flow distribution in automotive catalytic converters. *Applied Mathematical Modelling*, 28(9):775-794, 2004.

[28] W. Guojiang and T. Song. CFD simulation of the e ect of upstream flow distribution on the light-off performance of a catalytic converter. *Energy Conversion and Management*, 46(1314):2010-2031, 2005.

[29] S. Tischer and O. Deutschmann. Recent advances in numerical modeling of catalytic monolith reactors. *Catalysis Today*, 105(34):407-413, 2005.

[30] C. Ozhan, D. Fuster, and P. Da Costa. Multi-scale flow simulation of automotive catalytic converters. *Chemical Engineering Science*, 116(0):161-171, 2014.

[31] S. Quadri. The effect of oblique entry into an automotive catalyst on the flow

distribution within the monolith. PhD thesis, Coventry University, 2008.

[32] A. Holmgren, T. Gronstedt, and B. Anderson. Improved flow distribution in automotive monolithic converters. *React. Kinet. Catal. Lett,* 60(2):363-371, 1997.

[33] F. Ekstrom and B. Andersson. Pressure drop of monolithic catalytic converters exper-iments and modeling. *SAE Technical paper,* Paper 2002-01-1010, 2002.

[34] R.E. Hayes and S.T. Kolaczkowski. Mass and heat transfer effects in catalytic monolith reactors. *Chemical Engineering Science*, 49(21):3587-3599, 1994.

[35] O.Deutschmann R. Schmidt, F. Behrendt, and J. Warnatz. Numerical modeling of catalytic ignition. *J. Symposium (International) on Combustion*, pages 1747-1754, 1996.

[36] A. Martin, N. Will, A. Bordet, P. Cornet, and P. et al. Effect of flow distribution on emissions performance of catalytic converters. *SAE Technical Paper*, Paper 980936, 1998.

[37] S. Jeong and W. Kim. A numerical approach to investigate transient thermal and conversion characteristics of automotive catalytic converters. *SAE Technical Paper*, Paper 980881, 1998.

[38] S. Jeong and W. Kim. Three-dimensional numerical study on the use of warm-up catalyst to improve light-off performance. *SAE Technical Paper*, Paper 2000-01-0207, 2000.

[39] S. Mazumder and D. Sengupta. Sub-grid scale modeling of heterogeneous chemical reactions and transport in full-scale catalytic converters. *Combustion and Flame*, 131(12):85-97, 2002.

[40] V.K. Chakravarthy, J.C. Conklin, C.S. Daw, and E.F. DAzevedo. Multi-dimensional simulations of cold-start transients in a catalytic converter under steady in flow conditions. *Applied Catalysis A: General*, 241(12):289-306, 2003.

[41] S.E. Voltz, C.R. Morgan, D. Liederman, and S.M. Jacob. Kinetic study of carbon monoxide and propylene oxidation on platinum catalysts. *Industrial and Engineering Chemistry Product Research and Development*, 12(4):294-301, 1973.

[42] J J. Windmann, J. Braun, P. Zacke, and S. Tischer. Impact of the inlet flow distribution on the light-off behavior of a 3-way catalytic converter. *SAE Technical Paper,* Paper 2003-01-0937, 2000.

[43] B. Campbell, A. Finch, P. Tancell, and A. Hitchings. Effect of catalyst inlet cone flow mal-distribution on emissions performance of a close-coupled catalytic converter. *SAE Technical Paper*, Paper 2004-01-1489, 2000.

[44] S. Shuai and J. Wang. Unsteady temperature fields of monoliths in catalytic converters. *Chemical Engineering Journal*, 100(13):95-107, 2004.

[45] S. Mazumder. Modeling full-scale monolithic catalytic converters: Challenges and possible solutions. *Journal of Heat Transfer*, 129, Supplement(4):526-535, 2006.

[46] A. Kumar and S. Mazumder. Toward simulation of full-scale monolithic catalytic converters with complex heterogeneous chemistry. *Computers and Chemical Engineering*, 34(2):135-145, 2010.

[47] R.E. Hayes, B. Liu, R. Moxom, and M. Votsmeier. The effect of washcoat geometry on mass transfer in monolith reactors. *Chemical Engineering Science*, 59(15):3169 - 3181, 2004.

[48] R.E. Hayes, B. Liu, and M. Votsmeier. Calculating e ectiveness factors in non-uniform washcoat shapes. *Chemical Engineering Science*, 60(7):2037-2050, 2005.

[49] H. Yamamoto, H. Horie, J J. Kitagawa, and M. Minoru. Reduction of wall thickness of ceramic substrates for automotive catalysts. *SAE Technical Paper*, Paper 900614, 1990.

[50] B. Pfalzgraf, M. Reiger, and G. Ottowitz. Close-coupled catalytic converters for compliance with lev/ulev and eg iii legislation - influence of support material, cell density and mass on emission results. *SAE Technical Paper*, Paper 960261, 1996.

[51] K. Umehara, T. Yamada, T.Hijikata, Y. Ichikawa, and F. Katsube. Advanced ceramic substrate: Catalytic performance improvement by high geometric surface area and low heat capacity. *SAE Technical Paper*, Paper 971029, 1997.

[52] K.W. Hughes, D. Gian, and J. Calleja. Relative benefits of various cell density ceramic substrates in different regions of the ftp cycle. *SAE Technical Paper*, Paper 2006-01-1065, 2006.

[53] K.W. Hughes and W. Witte. Ultra-thin wall substrates - trends for performance in ftp and us06 tests. *SAE Technical Paper*, Paper 2002-01-0356, 2002.

[54] T. Leonhard, P. Floerchinger, A. Degen, W. Held, S. Hinze, and E. Pott. Effect of cell geometry on emissions performance of ceramic catalytic converters. *SAE Technical Paper*, Paper 2002-01-0354, 2002.

[55] K.W. Hughes, K. M. Schmitz, D.A. Radke, K. Zerafa, and B. Light. Impact of ultra thinwall catalyst substrates for tier2 emission standards. *SAE Technical Paper*, Paper 2003-01-0658, 2003.

[56] K. Umehara, M. Makino, M. Brayer, E.R. Becker, and R. Watson. Prediction of catalytic performance for ultra-thin wall and high cell density substrates. *SAE Technical Paper,* Paper 2000-01-0494, 2000.

[57] J. Gong, L. Cai, W. Peng, J. Liu, Y. Liu, H. Cai, and E. Jiaqiang. Analysis to the impact of monolith geometric parameters on emission conversion performance based on an improved three-way catalytic converter simulation model. *SAE Technical Paper*, Paper 2006-32-0089, 2006.

[58] H. Lun, N. Xiaowei, Z. Liang, L. Yongping, and H. Wei Z. He. CFD simulation of the e ect of monolith wall thickness on the light o performance of a catalytic converter. *International Journal of Chemical Reactor Engineering*, 8(1):Article A37, 2010.

[59] William S. Meisel and D.C. Collins. Repro-modeling: An approach to efficient model utilization and interpretation. *Systems, Man and Cybernetics*, IEEE Transactions on, SMC-3(4):349-358, 1973.

[60] T. Turanyi. Application of repro-modeling for the reduction of combustion mechanisms. *Symposium (International) on Combustion*, 25(1):949-955, 1994. Twenty-Fifth Sym-posium (International) on Combustion.

[61] T. Turanyi. Parameterization of reaction mechanisms using orthonormal polynomials. *Computers and Chemistry*, 18(1):45-54, 1994.

[62] A.Bukiand, T.Perger, T.Turanyi, and U.Maas. Repro-modelling based generation of intrinsic low-dimensional manifolds. *Journal of Mathematical Chemistry*, 31(4):345-362, 2002.

[63] M. Votsmeier. Efficient implementation of detailed surface chemistry into reactor models using mapped rate data. *Chemical Engineering Science,* 64(7):1384-1389, 2009.

[64] A. Scheuer, O. Hirsch, R. Hayes, H. Vogel, and M. Votsmeier. Efficient simulation of an ammonia oxidation reactor using a solution mapping approach. *Catalysis Today*, 175(1):141-146, 2011. The 6th International Conference on Environmental Catalysis (6th ICEC) Beijing, China, September 12-15, 2010.

[65] A. Scheuer, A. Drochner, J. Giesho , H. Vogel, and M. Votsmeier. Runtime efficient simulation of monolith catalysts with a dual-layer washcoat. *Catalysis Today*, 188(1):70-79, 2012. Modeling of Exhaust-Gas After-Treatment.

[66] M. Votsmeier, A. Scheuer, A. Drochner, H. Vogel, and J. Giesho . Simulation of automotive NH3 oxidation catalysts based on pre-computed rate data from mechanistic surface kinetics. *Catalysis Today*, 151(34):271-277, 2010. Diesel emissions control catalysis.

[67] A. Fadic, T. Nien, J. Mmbaga, R.E. Hayes, and M. Votsmeier. A case study in multi-scale model reduction: The effect of cell density on catalytic converter performance. *The Canadian Journal of Chemical Engineering*, 92(9):1607-1617, 2014.

[68] D. Goodwin. Cantera: An object-oriented software toolkit for chemical kinetics, thermodynamics, and transport processes. Caltech, Pasadena, 2009.